Harmful Algae
March 2021, Volume 103 Pages 102010 (17p.)
https://doi.org/10.1016/j.hal.2021.102010
https://archimer.ifremer.fr/doc/00693/80484/

Niche differentiation of *Dinophysis acuta* and *D. acuminata* in a stratified fjord

Baldrich Ángela M. [1, 10, *] , Pérez-Santos Iván [2, 3], Álvarez Gonzalo [4, 5], Reguera Beatriz [6], Fernández-Pena Concepción [7], Rodríguez-Villegas Camilo [1, 10], Araya Michael [5], Álvarez Francisco [5], Barrera Facundo [8], Karasiewicz Stephane [9], Díaz Patricio A. [2, 10]

[1] Programa de Doctorado en Ciencias, mención Conservación y Manejo de Recursos Naturales, Universidad de Los Lagos, Camino Chinquihue km 6, Puerto Montt, Chile
[2] Centro i~mar, Universidad de Los Lagos, Casilla 557, Puerto Montt, Chile
[3] Centro de Investigación Oceanográfica COPAS Sur-Austral, Universidad de Concepción, Chile
[4] Departamento de Acuicultura, Universidad Católica del Norte, Coquimbo, Chile
[5] Centro de Investigación y Desarrollo Tecnológico en Algas (CIDTA), Universidad Católica del Norte, Coquimbo, Chile
[6] Centro Oceanográfico de Vigo, Instituto Español de Oceanografía (IEO), Vigo, Spain
[7] Centro Oceanográfico de A Coruña, Instituto Español de Oceanografía (IEO), A Coruña, Spain
[8] Center for Climate and Resilience Research (CR2), Facultad de Ciencias Naturales y Oceanográficas Universidad de Concepción & Departamento de Química Ambiental Universidad Católica de la Santísima Concepción, Concepción, Chile
[9] Laboratory of Environment Resources, Boulogne- sur- Mer, French Research Institute for the Exploitation of the Sea (IFREMER), Issy-les-Moulineaux, France
[10] CeBiB, Universidad de Los Lagos, Casilla 557, Puerto Montt, Chile

* Corresponding author : Angela M. Baldrich, email address : ambaldrich@gmail.com

Abstract :

Dinophysis acuta and D. acuminata are associated with lipophilic toxins in Southern Chile. Blooms of the two species coincided during summer 2019 in a highly stratified fjord system (Puyuhuapi, Chilean Patagonia). High vertical resolution measurements of physical parameters were carried out during 48 h sampling to i) explore physiological status (e.g., division rates, toxin content) and ii) illustrate the fine scale distribution of D. acuta and D. acuminata populations with a focus on water column structure and co-occurring plastid-bearing ciliates. The species-specific resources and regulators defining the realized niches (sensu Hutchinson) of the two species were identified. Differences in vertical distribution, daily vertical migration and in situ division rates (with record values, 0.76 d−1, in D. acuta), in response to the environmental conditions and potential prey availability, revealed their niche differences. The Outlying Mean Index (OMI) analysis showed that the realized niche of D. acuta (cell maximum 7 × 103 cells L−1 within the pycnocline) was characterized by sub-surface estuarine waters (salinity 23 – 25), lower values of turbulence and PAR, and a narrow niche breath. In contrast, the realized niche of D. acuminata (cell maximum 6.8 × 103 cells L−1 just above the pycnocline) was characterized by fresher (salinity 17 – 20) outflowing surface waters, with higher turbulence and light intensity and a wider niche breadth. Results from OMI and PERMANOVA analyses of co-occurring microplanktonic ciliates were compatible with the hypothesis of species such as those from genera Pseudotontonia and Strombidium constituting an alternative ciliate prey to Mesodinium. The D. acuta cell maximum was associated with DSP (OA and

DTX-1) toxins and pectenotoxins; that of D. acuminata only with pectenotoxins. Results presented here contribute to a better understanding of the environmental drivers of species-specific blooms of Dinophysis and management of their distinct effects in Southern Chile. Previous article

Highlights

► 48 h of high frequency physical data for co-occurring blooms of 2 *Dinophysis* species. ► *D. acuta* (exceptional μ) thin layer briefly disrupted by an increase in turbulence. ► Co-occurring *D. acuminata* and *D. acuta* blooms showed a clear niche differentiation. ► Niche analysis results compatible with putative ciliate prey other than *Mesodinium*. ► *D. acuta* maximum associated with DSP toxins (OA, DTX1), *D. acuminata* with PTX2 only.

Keywords : *Dinophysis acuminata*, *Dinophysis acuta*, Realized niche, in situ division rates, Microplanktonic ciliate prey, DSP toxins, Pectenotoxins, Chilean fjords

1. Introduction

Species of *Dinophysis* have drawn attention worldwide due to their capacity to produce two groups of lipophilic toxins. The first group, okadaic acid (OA) and its derivatives, the dinophysistoxins (DTX), cause diarrhetic shellfish poisoning (DSP) (Gestal-Otero, 2014; Reguera et al., 2014; Yasumoto et al., 1980); the second group, the pectenotoxins (PTX), are hepatotoxic in cellular assays (Munday, 2014), and cause negative effects on early life stages of fish (Rountos et al., 2019) and shellfish (Gaillard et al., 2020). The production of one or both groups of toxins is very variable, even between strains of the same species from different regions (Reguera et al., 2014).

Accumulation of *Dinophysis* toxins, even at low cell densities (10^2-10^3 cells L^{-1}), by filter-feeding bivalves may exceed seafood safety regulatory thresholds (160 µg OA equiv. kg^{-1} meat) (European Commission, 2019) and cause lengthy harvesting quarantines. The impact of *Dinophysis* blooms is affected by the toxic potential of the local strains of *Dinophysis*, i.e., toxin profile and content, and by the specific transformation of the toxins by each shellfish species (Blanco et al., 2018). The main species which cause shellfish toxicity in western Europe are *Dinophysis acuminata* and to a lesser extent *D. acuta* (Fernández et al., 2019; Reguera et al., 2014; Swan et al., 2018).

Earlier studies in Chilean fjords focused on general aspects of the phytoplankton communities, including *Dinophysis* species (Avaria, 2008; Cassis et al., 2002; Pizarro et al., 2018; Seguel et al., 2005); the relationship of *Dinophysis* populations with environmental conditions (Alves-de-Souza et al., 2019; Alves-de-Souza et al., 2014; Díaz et al., 2011; Muñoz, 1992); and the detection and quantification of *Dinophysis* toxins in the framework of monitoring programmes (Fux et al., 2011; García et al., 2004; Pizarro et al., 2011; Uribe et al., 2001). These studies showed that *Dinophysis acuta* and *D. acuminata* are frequently

recorded in the southernmost regions in recent decades, and that their blooms pose a threat to public health, artisanal fisheries and the mussel industry. However, little is known about their species and site-specific requirements and the contribution of each species to toxic outbreaks (Díaz et al., 2019a).

Dinophysis species are obligate kleptoplastidic mixotrophs. They require ciliate prey (e.g., *Mesodinium*), light and nutrients for sustained growth (Kim et al., 2012; Kim et al., 2008; Park et al., 2006). Other plastid-bearing ciliate genera, such as *Cyrotostrombidium, Laboea* and *Strombidium* have been suggested as potential alternative prey (Kim et al., 2012; Stoecker et al., 2009). Field studies have shown that each *Dinophysis* species or even strain has different environmental windows for growth (Escalera et al., 2006; Maestrini, 1998). Thus, *D. acuminata* is considered a cosmopolitan species distributed over a wide range of salinity and temperature, while *D. acuta* is a temperate water species usually found in narrow ranges for these two environmental variables (Moita et al., 2006; Reguera et al., 2012). Results from Galician-Portuguese coastal waters reveal that when *D. acuminata* and *D. acuta* co-occur, they are vertically segregated with their cell maxima in different water masses (Díaz et al., 2019b; Escalera et al., 2006). These observation suggested that the two species have different physiological and behavioural adaptations. Laboratory culture studies confirmed the different responses of the two species to light intensity and quality (García-Portela et al., 2018; Kim et al., 2008), turbulence (García-Portela et al., 2019) and nitrogen sources (García-Portela et al., 2020; Hattenrath-Lehmann and Gobler, 2015).

A detailed understanding of the site and strain specific factors that trigger HAB development is needed to model their population dynamics and prevent or minimize their negative consequences (GEOHAB, 2011). Dinoflagellate blooms, in particular those of *Dinophysis* species, are often associated with stratified conditions (GEOHAB, 2008).

Fjords are highly stratified systems, and the persistence and strength of stratification appears to be one of the most important conditions for *Dinophysis* bloom development (Raine et al., 2018; Roy et al., 2018). A key question is to identify the microstructure characteristics of a given stratified system, i.e., temperature and salinity gradients, and pycnocline depths, that select a determined species' strain. High resolution measurements of the vertical distribution of physical and chemical properties of the water column are needed, as well as an evaluation of the physiological status of the cells (*in situ* division rate) and prey availability. These measurements allow distinction between actively dividing or recently advected senescent cells of the target species and descriptions of their behaviour.

The Hutchinson concept of ecological niche (Hutchinson, 1957) is a useful approach to understand the relationship between a species distribution and its environment (Colwell and Rangel, 2009; Holt, 2009; Pagel and Schurr, 2012). Hutchinson postulates two components for the ecological niche of a given species. First, the fundamental niche: the *n*-dimensional hypervolume within which the population of a species can persist, survive, and reproduce indefinitely. The fundamental niche is not constrained by any biological interactions. Second, the realized niche, i.e., the proportion of the fundamental niche within which the species actually persists. The realized niche takes into account the effect of abiotic variables and biological interactions (Hutchinson, 1957). This niche perspective has been applied to the study of different groups of phytoplankton both in laboratory (fundamental niche) and field (realized niche) conditions (Brun et al., 2015; Irwin et al., 2012; Litchman et al., 2012). The Outlying Mean Index (OMI) analysis proposed by Dolédec et al. (2000) is a useful ordination method for describing phytoplankton species niches (Grüner et al., 2011; Hernández-Fariñas et al., 2015; Sutani et al., 2014), including those responsible for HAB events (Alves-de-Souza et al., 2019; Karasiewicz et al., 2018; Karasiewicz et al., 2020).

During late summer (February) 2019, high density blooms of *D. acuminata* and *D. acuta* co-occurred in Southern Chile, offering an opportunity to undertake a detailed niche partitioning study. In the present study, results were analysed from the niche perspective, using the Outlying Mean Index (Dolédec et al., 2000). *In situ* measurements were made of division rates and toxin content of both *Dinophysis* species during two daily cycles, and of daily vertical migration and distribution in relation to potential ciliate prey. The hypothesis was that different physiological and behavioural traits determine bloom development success of *D. acuminata* and *D. acuta* under a distinct set of conditions (realized niche) when they co-occur in stratified fjords. The main objective was to identify the environmental variables, during 48 h intensive sampling, which define the realized niche of *D. acuta* and *D. acuminata* and explain their microscale distribution in Puyuhuapi Fjord.

2. Materials and Methods

2.1. Study area

Puyuhuapi Fjord (PF), Aysén Region, northern Patagonia (~44°50´S; Fig. 1) is 100 km long with a N-NE orientation. The fjord is connected to Moraleda Channel at the mouth and with Jacaf Channel close to the head in a region with extremely high (~3,500 - 4000 mm yr^{-1}) precipitation (Sauter, 2020). The main freshwater input is the Cisnes River (average streamflow 218 m^3s^{-1}), which flows into the middle part of the fjord (Schneider et al., 2014). Smaller rivers Ventisquero (average streamflow 40 m^3s^{-1}), Marta and Uspallante (no data available) also discharge freshwater into this fjord (Calvete and Sobarzo, 2011).

Waters from the northern area of PF are more brackish than those from the southern area except in winter, when this pattern may be reversed due to the intrusion of oceanic water through Jacaf Channel, and vertical stratification is very variable (Schneider et al., 2014).

The circulation is of two-layered estuarine-type, with a variable (5-10 m) estuarine surface layer (EW) and a more uniform saltier lower layer, the Subantarctic Water (SAAW, salinities > 33) reaching 150 m depth (Silva and Calvete, 2002). Mixing at the interface of the two layers yields Modified Subantarctic Water (MSAAW, salinities 31 to 33) (Schneider et al., 2014). Depending on the freshwater contribution, different water masses in the PF (as well as other fjords and channels in Patagonia) can be identified in the top layer: the Estuarine Fresh Water (EFW, with salinities 11 to 21) and the Estuarine Saline Water (ESW, with salinities 21 to 31). When salinity is less than 11, the water is classified as Fresh Water (FW) (Pérez-Santos et al., 2014).

2.2. Field sampling

High vertical resolution measurements of physical parameters were carried out during a 48 h cell cycle study of *Dinophysis* species and distribution of co-occurring plastid-bearing micro-ciliates. A fixed station was sampled from 26 to 28 February 2019 in PF. This fjord, the only one in the region with two connections with the open sea, has the highest water residence time (Díaz et al., 2021). It was selected as a hot spot of *Dinophysis* blooms and DSP outbreaks in Southern Chile according to the official monitoring data (IFOP) over the last ten years (data not shown). Vertical profiles of temperature, salinity, and in vivo chl *a* fluorescence were obtained with an AML Oceanographic CTD profiler (http://www.amloceanographic.com) model Metrec-XL equipped with a Turner Designs CYCLOPS-7 fluorometer (excitation 460 nm, emission 620-715 nm). This fluorescence sensor outputs an analog voltage proportional to the chl *a* concentration. CTD fluorescence data from a northern Patagonian fjord (41.6°S / 72.85°W) and chl *a* in bottle samples collected at standard depths (0, 5, 10, 15, 25, 50, 75, 100, 150, and 200 m) were highly

correlated (R^2=0.987) and used to convert the CYCLOPS-7 output voltage into chl *a* concentration. The (CTD) probe was cast every 2 h from the surface to 50 m depth. Vertical distributions of turbulence microstructure were measured with a Self-Contained Autonomous Micro Profiler (SCAMP) (100 Hz). Processing of the CTD and SCAMP data was carried out with the software provided by the manufacturer and depicted using the Ocean Data View software version 5.1 (Schlitzer, 2019). A Photosynthetically Active Radiation (PAR) sensor was used to obtain radiation data at the same sampling rate as the temperature and conductivity sensors. The turbulent kinetic energy dissipation rate (ε, m^2 s^{-3}) was estimated by applying the Batchelor spectrum to the vertical gradients of temperature (Luketina and Imberger, 2001).

Plankton nets (20 µm mesh) were towed vertically from 20 m to the surface every hour and aliquots of 100 mL fixed with neutral Lugol's iodine solution (Lovegrove, 1960) to estimate *in situ* daily average division rates (µ) of the two species, as in Velo-Suárez et al. (2009). For quantitative analysis of *Dinophysis* species and their potential microciliate prey, water samples of 100 mL, were collected every 2 h at 2 m intervals, from 0 to 20 m, and at 25 m and 30 m with 5 L Niskin bottle, and fixed with neutral Lugol's iodine solution (Lovegrove, 1960). In addition, 2 L samples were collected at each depth on 27 and 28 February 2019 to estimate division rates at specific depths $(\mu_{min})_z$ and the depths where the maximal values of $(\mu_{min})_z$ were estimated. These samples were collected at 10:00 h LT, the time of day when maximal cell division of *D. acuta* was expected, filtered through 20 µm nytex filter and re-suspended in 50 mL of seawater with Lugol´s iodine solution, a protocol used to increase counting resolution of *D. acuta* and *D. acuminata* as in Velo-Suárez et al. (2009).

For toxin analyses, bottle samples were collected every 2 h at 4 m intervals from surface to 20 m (6 fixed depths), and 1 L aliquots filtered through Whatman GF/F fiberglass filters (25 mm Ø, 0.7 µm pore size) (Whatman, Maidstone, England). The filters and filtered material were placed in a cryotube, mixed with 1 mL analysis grade methanol and stored in the laboratory at −20°C until analysis. The field sampling is summarized in Fig. S1.

2.3. Nutrient analyses

Water samples for inorganic nutrient (NO_3^-, NO_2^-, PO_4^{3-}, and Si $(OH)_4$) analyses were taken three times throughout the 48 h sampling, using 50 mL syringes directly connected to the spigot of the Niskin bottle at each sample depth (i.e., 2, 5, 10, 15, 20 and 50 m). Dissolved inorganic nutrients were analysed with a Seal AA3 AutoAnalyzer, as in Grasshoff et al. (1983) and according to standard methods for seawater analysis (Kattner and Becker, 1991). Ammonia analyses were omitted for logistic reasons, i.e., the impossibility to ensure analyses of this labile molecule very soon after collection in remote areas in southern Chile.

2.4. Phytoplankton analyses

Sedimentation chambers of 10 mL were used to sediment aliquots of each Lugol-fixed bottle sample. Samples were left to sediment for 24 h for quantitative analyses of *Dinophysis* species and ciliates with inverted microscopes Olympus CX40 (Olympus, Japan) and Nikon Eclipse TE300 (Nikon, Japan) respectively, according to Utermöhl (Utermöhl, 1958). To count *Dinophysis* species and ciliates, the whole surface of the chamber was scanned at a magnification of x100, so that the detection limit was 100 cells L^{-1}. Ciliates were identified to genus, or to species level when possible using

magnifications of x200 and x400. Taxonomic nomenclature complied with the World Register of Marine Species (WORMS, http://www.marinespecies.org/, last access June 10th, 2020).

2.5. Division rates

Aliquots (1 mL) of each Lugol-fixed net haul and concentrated 2 L bottle samples were analysed using Sedgewick-Rafter counting slides with an inverted microscope (Olympus CX40). Net haul samples were used to get the daily average specific division rate (μ) of *D. acuta* and *D. acuminata* in the water-column (0 - 20 m). Two cell cycle stages of each species were counted-dividing (paired cells) and recently divided cells (incomplete development of the left sulcal list). These stages were considered as terminal events to estimate *in situ* division rates with a post-mitotic index (Reguera et al., 2003) adapted from the mitotic index model of Carpenter and Chang (1988). Vegetative or asexual division in *Dinophysis* occurs by desmoschisis. In the division process, the two daughter cells remain attached by their dorsal margins in an intercalary growth zone, the dorsal megacytic bridge, forming cell pairs (*p*) that remain together for a period of time that varies among *Dinophysis* species and according to dominant environmental conditions. The sulcal lists of the mother cells are not evenly distributed. This is an easily distinguished morphological character to recognize the recently divided daughter cells (I_r). A minimum of 300 cells of each species (depending on their abundance in the field) was examined for each data point of the frequency graph. Frequencies (*f*) of cells undergoing mitosis (f_p) and of recently divided cells (f_r) at each sampling time were estimated according to:

$$f_p + f_r = \frac{p + \frac{I_r}{2}}{I_c + p + \frac{I_r}{2}}$$

where f_p = frequency of cell pairs; f_r = frequency of recently divided cells; I_c = fully developed (complete) cells. In all cases, examination was continued on samples collected during the hours of reproduction until at least 30 events (dividing cells) had been observed. The daily average division rate, μ, for each species and 24 h cycle was estimated according to the equation of Carpenter and Chang (1988):

$$\mu = \frac{1}{n(T_c+T_r)} \sum_{i=1}^{n} (t_s)_i \ln\left[1 + f_c(t_i) + f_r(t_i)\right]$$

The "maximum frequency approach" (McDuff and Chisholm, 1982) was applied to estimate the lower bound of the division rate (μ_{min}). The latter is a minimum estimate of the division rate and will approach the true value of μ only with specific conditions (i.e., when a population has very synchronised division, and it is possible to identify all the dividing or recently divided cells in a single sample).

2.6. Lipophilic toxin analysis

Lipophilic toxins were extracted from the filters by sonication with a Branson Sonic Power 250 sonifier (Danbury, CT, USA) as described in Álvarez et al. (2016). To analyse free okadaic acid (OA) and other lipophilic toxins, 0.5 mL aliquots were placed in amber vials and stored at -20°C until analysis. For the detection of esterified OA-group toxins, 0.5 mL aliquots were subjected to alkaline hydrolysis following the standard procedure of the EU Reference Laboratory for Marine Biotoxins (EURLMB, 2015). Phytoplankton toxins analysis was carried out according to Regueiro et al. (2011) with minor modifications (a

shorter column and allowing enough time for the elution of all the toxins) with a Dionex Ultimate 3000 UHPLC system (Thermo Fisher Scientific, Sunnyvale, CA, USA). Toxins detection was carried out with a high-resolution mass spectrometer Q Exactive Focus equipped with an electrospray interphase HESI II (Thermo Fisher Scientific, Sunnyvale, CA, USA) (Table S1). The presence of lipophilic toxins was confirmed by comparing the retention time, exact mass and fragmentation spectra with those of certified reference solutions from the National Research Council (NRC, Halifax Canada). Toxins were quantified by comparing the area of the peaks obtained in the chromatograms with those of the certified reference materials. The detection (LOD) and quantification (LOQ) limits of the LC-MS/MS method were 1.73 ng mL^{-1} and 3.82 ng mL^{-1} respectively, for OA, 1.67 ng mL^{-1} and 2.93 ng mL^{-1} for DTX-1, and 0.82 ng mL^{-1} and 1.90 ng mL^{-1} for PTX-2.

2.7. Data analysis

Data of *Dinophysis* and ciliate cell densities were log transformed (ln(x+1)) to reduce the effect of dominant species. Environmental variables were standardized as in Alves-de-Souza et al. (2017), to values between 0 and 1, based on the minimum and maximum values of each variable. Statistical analyses were made using *ade4* and *vegan* packages of the free CRAN repository from R software (R Core Team, 2019). All data were graphed using the Ocean Data View software (Schlitzer, 2019).

2.7.1. Niche analysis

Data were sorted into two matrices. The first contained biological variables: cell densities of *D. acuta*, *D. acuminata* and their potential prey (plastid-retaining ciliates); the second,

289 the environmental variables: water temperature, salinity, turbulence, PAR, and sampling
290 depths.
291 An Outlying Mean Index (OMI) analysis was used to characterize the niche position and
292 breadth of *D. acuta* and *D. acuminata* (Dolédec et al., 2000). The analysis was performed
293 using the function '*niche'* in the *ade4* package (Dray and Dufour, 2007). This function uses
294 the centred and scaled environmental dataset, and the ln-transformed matrix containing the
295 cell densities of taxonomic units. The OMI analysis is an ordination technique designed to
296 explicitly take into account the ecological niche of each species within a community, by
297 determining the marginality of a given species (Dolédec et al., 2000). The marginality
298 (OMI parameter) of a species corresponds to its realized niche position in an *n*-dimensional
299 space; OMI analysis seeks the combinations of environmental variables that maximize, for
300 the entire community, each species' marginality. The OMI parameter is defined as the
301 squared Euclidean distance between the mean habitat conditions used by a species and the
302 mean habitat conditions of the sampling domain, the latter defined on a temporal or spatial
303 scale (Hernández-Fariñas et al., 2015; Karasiewicz et al., 2017). In other words, the OMI
304 parameter is defined as the distance between the species niche position and the mean
305 environmental conditions which is also the average habitat used by the community (the
306 origin of the Euclidean space *G*). Species with high/low marginality values occur in
307 uncommon/common habitats respectively (Dolédec et al., 2000; Hernández-Fariñas et al.,
308 2015). The total inertia (proportional to the average marginality of species), quantifies the
309 influence of the environmental variables on the niche separation of the species (Dolédec et
310 al., 2000).
311 The OMI analysis gives information on species niche breadth with the tolerance parameter
312 (Tol). High and low tolerance values are associated with taxa which occur in wide ranges

313 (i.e., generalists), and limited ranges (i.e., specialist) of environmental conditions
314 respectively (Karasiewicz et al., 2017). Finally, the residual tolerance (RTol) quantifies the
315 information lost after dimensional reduction. This parameter assesses the reliability of the
316 environmental variables used to define the species niche (Dolédec et al., 2000; Karasiewicz
317 et al., 2017).
318 The statistical significance of the OMI analysis was tested using Monte Carlo permutations
319 included in the packages '*ade4*' (10,000 permutations) (Alves-de-Souza et al., 2019;
320 Karasiewicz et al., 2017). The test compares the observed species' marginality and the
321 simulated values, under the null hypothesis that each species is indifferent to its
322 environment (Dolédec et al., 2000).
323 To identify the relevance of the environmental variables (i.e., depth, temperature, salinity,
324 turbulence, PAR, and the cell density of different ciliates) for *D. acuta* and *D. acuminata*, a
325 marginal Permutational Analysis of Variance (PERMANOVA) based on Euclidean
326 distances was performed (Anderson, 2014). The analysis estimates an empirical (pseudo)
327 *F-value* for each term using 10,000 permutations, to test an association null hypothesis
328 between the *Dinophysis* species and environmental variables. The analysis was executed
329 with the function *adonis2* from the package 'vegan' (Oksanen et al., 2018) using the
330 statistical and programming software R (R Core Team, 2019).
331
332 **3. Results**
333 *3.1. Oceanographic conditions*
334 Oceanographic conditions during the 48 h sampling at a fixed station showed the
335 characteristic layering of the fjord described by Pérez-Santos et al. (2014) with an
336 intermittent temperature reversal at the surface. This layering is favoured by riverine

337 outflow of cold freshwater that was particularly high in the spring preceding this study (Fig.
338 2). Diurnal temperature variability in the upper 3 m ranged between 16 and 18 °C. This
339 variability was clearly linked to the daily solar heating, from 7:30 to 20:40, and formation
340 of a diurnal thermocline. Strong thermal gradients in the upper 10 m (from 18 to 14°C)
341 were maximal (0.5 °C m^{-1}) between 6 and 10 m. From 10 to 20 m, temperatures dropped
342 from 14 to 10 °C (Fig. 2A). Salinity values confirmed (according to the classification in
343 Pérez-Santos et al. (2014)), the presence of Estuarine Fresh Water (EFW, 17.3 to 21) on the
344 surface (0-4 m), Estuarine Salty Water (ESW, 21.19 to 31) below the EFW down to 15 m
345 with a maximal salinity gradient between 5 and 8 m, and Modified Subantarctic Water
346 (MSAAW, 31 to 33), with more uniform salinity, from 15 to 20 m (Fig. 2B). Strong
347 stratification in the upper 10 m was associated with high values of the Brunt-Väisälä
348 frequency that were maximal (60 - 90 cycles h^{-1}) in the inter-phase between the EFW and
349 the ESW (4 to 8 m) (Fig. 2C). Photosynthetically active radiation (PAR) was maximal (~
350 1000 µmol m^{-2} s^{-1}) the second day between 0 and 5 m from 11:00 to 16:00 h (Fig. 2D).
351 There were no relevant changes in the vertical distributions of inorganic nutrients, at the
352 beginning, mid-point and end of the study. Silicate concentration, with a maximum (> 8
353 µmol L^{-1}) at the surface (0 - 2 m) from the river input, dropped between 5 and 10 m and
354 increased again below 15 m. Nitrate and phosphate concentrations gradually increased with
355 depth, with maximum values of 15 and 2 µmol L^{-1}, respectively, in the subsurface layer (15
356 - 20 m). The highest nitrite concentrations (0.7 - 1.0 µmol L^{-1}) were detected between 5 and
357 15 m (Fig. 3).

3.2. *Vertical distribution of* Dinophysis, Mesodinium *and other potential prey*

3.2.1 *Distribution of* Dinophysis *in relation to physical parameters*

High cell densities of *D. acuta* and *D. acuminata* were mainly restricted to the upper layer (0 - 10 m), although populations of the two species were vertically segregated (Fig. 4B, C). *Dinophysis acuta* maximum (7.3 x 10^3 cells L^{-1}) was detected at 4 m, at 18:00 h on 26 February (Fig. 4B), i.e., at the depth where the salinity gradient (in the interface between EFW and ESW) and the Brunt-Väisälä frequency (Fig. 2C) were maximal. During the first 24 h, *D. acuta* migrated vertically (DVM) between 4 and 8 m, with the maximum closer to the surface at night (Fig. 4B). This DVM was different from the tidal signal during this time period (Fig. 4A). Between 16:00 h on February 27 and 2:00 h on February 28, *D. acuta* densities declined abruptly. This decline coincided with changes in the water column structure and increased turbulence ($\varepsilon < 10^{-6}$ m^2 s^{-3}). Numbers increased again from 2:00 h onwards, after the water column structure returned to the previous conditions, with maximal cell numbers at the depth of maximal density gradient.

In contrast, *D. acuminata*, was detected in very low numbers during the first 24 h, but much higher values appeared at the surface (0 - 2 m), between 20:00 h and 00:00 h the second day, coinciding with the *D. acuta* decline; it reached a maximum of 6.8 x 10^3 cells L^{-1} (Fig. 4C) in an almost isothermal (18°C) surface layer (Fig. 4B, C, E) at flood tide (Fig. 4A, C).

Plots of *D. acuta* and *D. acuminata* numbers on potential temperature-salinity (T-S) diagrams were significantly different (Fig. 5). High densities (> 3 x 10^3 cells L^{-1}) of *D. acuta* were found in the ESW water layer with a temperature range of 12.9 to 16.6°C and salinity 21.0 - 28.4, corresponding to $\sigma\theta$ values of 15 to 20. The cell maximum (>7 x 10^3 cells L^{-1}) was found within much narrower ranges of temperature (15.4 - 16.4°C) and

381 salinity (22.9-25.4) (Fig. 5A). High densities of *D. acuminata*, (> 3 x 10^3 cells L^{-1}) were
382 associated with the surface EFW water, with a temperature range of 16.1 to 16.5°C and
383 salinity 17.4 to 20.0. The cell maximum (6.8 x 10^3 cells L^{-1}) was recorded at 16.2°C and
384 salinity 17.4. Thus, high cell densities of *D. acuminata* were associated with less dense
385 water (σθ values between 12.5 and 15) than those where *D. acuta* maxima were found (Fig.
386 5B).
387
388 *3.2.2. Distribution of* Mesodinium *and other potential ciliate prey*
389 *Mesodinium* species, potential prey of *Dinophysis*, were the dominant microplanktonic
390 ciliates throughout the 48 h sampling. Maximum densities (9 x 10^3 cells L^{-1}) occurred in the
391 surface layer (0 - 2 m) between 20:00 h and 22:00 h during the second day of the study
392 (Fig. 4D), coinciding with those of *D. acuminata* (Figs. 4B-D). In contrast, there was no
393 overlap between *Mesodinium* and *D. acuta* cell maxima.
394 Other plastid-retaining ciliates, such as *Laboea* sp., *Strombidium* spp., *Leegaardiella* spp.,
395 *Cyrtostrombidium* spp., *Paratontonia* spp., *Pseudotontonia* sp. and *Lohmanniella* sp., were
396 detected, and some of them (e.g., *Lohmanniella* sp.) in high densities (Fig. 6; Table S2).
397 There were relevant differences between the distributions of these ciliates and those of *D.*
398 *acuta* and *D. acuminata.* However, there were some overlaps of *Dinophysis* with potential
399 alternative ciliate prey. For example, *D. acuta* maxima coincided with high densities (> 500
400 cells L^{-1}) of *Pseudotontonia* sp. between 2 and 8 m from 12:00 to 20:00 h in the first 24 h
401 (Fig. 4B and Fig. 6C), and with *Paratontonia* spp. in the upper 6 m from 8:00 to 12:00 h
402 the second day (Fig. 4B and Fig. 6F). Cell maxima (> 800 cells L^{-1}) of *Strombidium* spp.

coincided with those of *D. acuminata* in the upper 5 m, from 16:00 to 4:00 h the second day (Fig. 4C and Fig. 6B).

3.3. Physiological status of Dinophysis *cells*

Both species of *Dinophysis* exhibited high division rates ($\mu > 0.5$ d^{-1}) during the 48 h study, but their phased-cell division was not very synchronized. Division in both species began at dawn (6:00 h) and lasted until 14:00 h. Total frequency of mitotic cells did not show a single peak, with the exception of the cell cycle of *D. acuta* the first 24 h (Fig. 7).

The frequencies of dividing (f_c) and recently divided (f_r) cells of *D. acuta* revealed phased cell division on February 27; f_c and f_r maxima, less than 1 h apart, formed sharp peaks at 11:00 h, 5 h after sunrise (Fig 7A). Results were quite different the next day (February 28). There were two f_c peaks (at 8:00 h and 11:00 h); the f_r maximum was very close (< 1 h) to the first peak. Estimates of μ and μ_{min} were 0.57 d^{-1} and 0.45 d^{-1} on February 27 and 0.76 d^{-1} and 0.50 d^{-1} on February 28, respectively.

An f_c maximum of *D. acuminata* occurred at 10:00 h on February 27, one hour earlier than that in *D. acuta*; there were two smaller f_c peaks, one two hours earlier (at 8:00 h), the second two hours after (at 12:00 h) the maximum. Values of f_r had a similar pattern, with a first peak at 8:00 h, 3 h before the maximum at 11:00 h (Fig. 7B). The next day, f_c values formed a plateau from 8:00 to 12:00 h. The maximum value of f_r was at 8:00 h on the two sampling days. Estimates of μ and μ_{min} were 0.49 d^{-1} and 0.28 d^{-1} on February 27, and 0.54 d^{-1} and 0.30 d^{-1} on February 28, respectively (Fig. 7B).

Vertical profiles of $(\mu_{min})_z$ (i.e., μ_{min} at specific depths) at 10:00 h on February 27 and 28 showed that the maximal estimate of μ_{min} for each *Dinophysis* species was located at different depths within the pycnocline region (Fig. 8). For *D. acuta*, values of 0.39 d^{-1} and

427 0.34 d^{-1} co-occurred with cell maxima of 6.3 x 10^3 and 6.7 x 10^3 cells L^{-1}, respectively on
428 the two days, located in mid-pycnocline (6m), forming a well-defined thin layer the second
429 day (Fig. 8 A, B, E). Moderate densities of *D. acuminata* (maxima < 10^3 cells L^{-1} first day
430 and 1.1 x 10^3 cells L^{-1} second day) occurred in the two profiles at 10:00, with a cell
431 maximum the second day at 4 m, at the top of the pycnocline (Fig. 8 F); division rates were
432 lower than those of *D. acuta*, with a maximum of 0.27 d^{-1} the first day (Fig. 8 C). Values of
433 $(\mu_{min})_z$ were almost uniform with depth (from 2 to 12 m) the second day (maximum of 0.24
434 d^{-1}); no well-defined thin layer like that of *D. acuta* was observed (Fig. 8F).
435 Phytoplankton extracts contained diarrhetic toxins (OA, DTX-1) and pectenotoxins (PTX-
436 2) throughout the sampling period. Concentrations of OA and DTX-1 co-varied, and their
437 vertical distribution, with maximal values at 4 m, paralleled that of *D. acuta*, and were
438 under detection levels at 0 m (Fig. 9 A-C). Maximal concentrations of PTX-2 at 4 m and
439 8m coincided with maximal densities of *D. acuta*, but high values of PTX-2 were also
440 detected at 0 m, from 20:00 to 2:00 h the second day, when OA and DTX-1 were almost
441 zero. This PTX-2 maximum at 00:00, was associated with high values (4-7 x 10^3 cells L^{-1})
442 and an overwhelming dominance of *D. acuminata* (e.g., 84% at 00:00 and 96% at 2:00 on
443 the 2 m samples, Fig. 9A).
444
445 *3.4. Niche analysis*
446 The OMI analysis (Table 1) showed that the two species of *Dinophysis*, their putative prey
447 (*Mesodinium* spp.) and other potential alternative ciliate prey, had significant realized
448 niches ($p < 0.01$). The physical variables included in the analysis had significant influences
449 on most (8 out of 10) of the species included.

450 The first and second axis of the OMI ordination (PC1 and PC2) encompassed 82.24%
451 (OMI1: 63.88% and OMI2: 18.36%) of the total projected inertia (Fig. 10A). The OMI
452 plane was defined by two diagonal gradients, each one with inversely correlated variables
453 (Fig. 10B). The first gradient was characterized by Depth - Temperature from the top-left
454 (cold deep water) to the bottom-right (warm and shallow water) of the plan. The second
455 gradient was characterized by Salinity – Turbulence - PAR from the bottom-right (saltier
456 water with lower turbulence and light intensity) to the top-left (fresher estuarine waters
457 with higher turbulence and light intensity) of the plan. The PERMANOVA analysis for
458 *Dinophysis* species and physical parameters (depth, temperature, salinity, turbulence, and
459 PAR), showed that temperature, salinity and PAR were the significant variables ($p < 0.05$)
460 that contributed to most of the explained variability of *Dinophysis* species. In addition,
461 turbulence had a *p-value* = 0.08 (Table 2).
462 Most of the species were distributed along the Depth - Temperature gradient (Fig. 10B).
463 The OMI analysis showed that the niches of the two *Dinophysis* species and most of the
464 ciliates, were characterized by habitat preferences (*sensu* ter Braak and Verdonschot 1995)
465 for upper layers of the water column, but they differed from each other in salinity,
466 temperature, turbulence and PAR preferences. The niches of the two *Dinophysis* species
467 were quite distinct. That of *D. acuta* was mainly defined by sub-surface waters, influenced
468 by relatively high temperatures, low salinity, and a tendency to avoid conditions of higher
469 turbulence and PAR. On the other hand, the niche of *D. acuminata* was located in more
470 variable estuarine surface waters with higher turbulence and PAR (Fig. 10B). In addition,
471 *D. acuta* had a lower marginality value (OMI=0.65) than *D. acuminata* (OMI=1.83), due to
472 its wider distribution in the water column during the sampling period. Nevertheless, *D.*
473 *acuminata* showed a higher tolerance value (Tol=1.90) than *D. acuta* (Tol= 1.49),

474 indicating that the realized niche breadth of *D. acuta* was narrower than that of *D.*
475 *acuminata* (Table 1, Fig. 10C). *Mesodinium* (*Dinophysis* potential prey), had a low
476 marginality (OMI=0.10) and a very high niche breath (Tol=3.11), indicating that it could be
477 present through the habitat occupied by the two species of *Dinophysis* (Table 1, Fig. 10C).
478 Finally, PERMANOVA analysis of *Dinophysis* species and the plastid-retaining ciliates
479 included in the OMI analysis revealed that *Mesodinium* spp., *Pseudotontonia* sp. and
480 *Strombidium* spp., were significant factors explaining *Dinophysis* species abundance (Table
481 S3).
482
483 **4. Discussion**
484 During late summer (February) 2019, actively dividing populations of *Dinophysis*
485 *acuminata* and *D. acuta* co-occurred in PF. The co-occurrence of the two species brought a
486 unique opportunity to study their microscale distribution, behaviour, and potential
487 alternative ciliate prey. The main objective of the study was to elucidate how two species
488 expected to consume the same prey (the ciliate *Mesodinium*) could thrive blooming at the
489 same time and place. High vertical resolution physical measurements and biological
490 observations during an intensive 48 h cell cycle study at a fixed station in PF were analysed
491 with a realized niche (*sensu* Hutchinson 1957) approach. These results showed that the
492 spatial and temporal distribution of the two *Dinophysis* species, as well as their cell cycle,
493 responded differently to the environmental conditions and prey availability. In other words,
494 the niches of the two species were spatially and temporally differentiated. These results will
495 help to identify environmental conditions favouring bloom development of *D. acuta* and *D.*
496 *acuminata* in the Chilean fjords. In addition, the two species maxima were associated with
497 distinct toxin profiles: the profile of *D. acuta* was dominated by diarrhetic toxins, and that

498 of *D. acuminata* only with pectenotoxins. These two profiles have distinct impacts on
499 seafood safety management of commercial shellfish species in Chile (Blanco et al., 2018).
500
501 *4.1. Vertical distribution of* Dinophysis *species*
502 This study showed the co-occurrence of bloom (> 10^3 cells L^{-1}) densities of *D. acuta* and *D.*
503 *acuminata*, during 48 h sampling, but with differences in their vertical distributions. High
504 densities (> 3 x 10^3 cells L^{-1}) of *D. acuta* were found between 4 and 8 m in the pycnocline
505 (Fig. 4B), while those of *D. acuminata* were found in the upper 2 m (Fig. 4C). Studies in
506 Spain and Portugal have shown that when *D. acuminata* and *D. acuta* co-occurred, their
507 cell maxima were in water layers with different properties (Escalera et al., 2010; Palma,
508 1998; Reguera et al., 1993).
509 Water column stratification has been described as a main factor promoting dinoflagellate
510 bloom development, including *Dinophysis* blooms (Díaz et al., 2019b; Maestrini, 1998;
511 Reguera et al., 2012; Smayda, 2002). Maximal stratification in PF is observed during
512 spring-summer due to the contribution of the Cisnes River (Calvete and Sobarzo, 2011;
513 Schneider et al., 2014). Our results show strong density gradients, mainly in the top 10 m,
514 where all *Dinophysis* maxima were found. These gradients (Fig. 2A, B, C) result from the
515 permanent haline stratification of the fjord due to i) high ice-melt in spring from Cisnes
516 River exceeding 1500 m^3s^{-1} (http://chonos.ifop.cl/aguadulce/visor) and ii) positive SST
517 anomalies from high insolation in summer 2019. The distributions of the two species
518 suggest differential use of resources determined by their species-specific adaptations, which
519 can be translated into niche differentiation.
520 The OMI analysis shows that the environmental variables included in the analysis (i.e.,
521 depth, temperature, salinity, irradiance PAR and turbulence) can define the niches of the

two *Dinophysis* species. Their realized niches were characterized by their locations in the upper layers of the water column, but they differed from each other in salinity, temperature, turbulence, and PAR preferences. The OMI marginality results (low for *D. acuta* and higher for *D. acuminata*) (Table 1), indicate that these conditions represent the typical habitat of *D. acuta*, but atypical conditions for *D. acuminata* (Dolédec et al., 2000). In other words, the environmental conditions were more favourable for *D. acuta* most of the time, allowing a major occurrence of this species. In addition, it seems that *D. acuminata*, despite having a broader realized niche breadth than *D. acuta* (with high OMI and TOL) did not benefit from these conditions, except during the last hours of the study.

Field and laboratory studies have shown that temperature and salinity are relevant oceanographic factors for *Dinophysis* species in helping to explain their zonation (littoral, neritic, oceanic) and biogeography (cold, temperate, tropical), as well as their distribution in the water column (Maestrini, 1998; Reguera et al., 2014). In the Patagonian channels and fjords (including PF), salinity is the overwhelming property determining seawater density, and water masses are normally described mostly based on salinity values (Pickard, 1971; Sievers and Silva, 2008). Our results demonstrate the fundamental role of temperature in addition to salinity to explain the presence and cell densities of the two *Dinophysis* species. This is also shown by the OMI and PERMANOVA results. A clear vertical differentiation in the presence of *D. acuta* and *D. acuminata* was found. This differentiation separates the niches of the two species into water layers with different properties as described in Sievers and Silva (2008). The realized niche of *D. acuta* was mainly defined by the sub-surface more saline waters and a strong influence of temperature, whereas that of *D. acuminata* was in shallower, more estuarine waters (Fig. 10B). The highest densities of *D. acuta* occurred in the ESW subsurface layer (15 – 20 isopycnals) and highest values of *D. acuminata* in the

546 EFW surface water (12.5 - 15 isopycnals) (Fig. 5A, B). Observations in this study agree
547 with those from other systems subjected to blooms of *D. acuminata* and *D. acuta*, i.e., *D.*
548 *acuminata* is found within broader ranges of temperature and salinity than *D. acuta*. The
549 latter is a temperate to cold-temperate species that thrives in frontal areas when
550 temperature-driven stratification is maximal (late summer) (Paterson et al., 2017; Reguera
551 et al., 2014). Nevertheless, it is important to highlight the large intra-specific differences
552 related to the optimal temperature and salinity conditions for growth in different parts of the
553 world. For example, *D. acuta* blooms in NW Iberia are found in shelf waters with salinities
554 > 35 (Escalera et al., 2010; Moita et al., 2006) but the same species peaks in the Chilean
555 fjords at much lower salinities (15.2) (Díaz et al., 2011). *D. acuminata* blooms in the Baltic
556 Sea at 7.0°C and salinity 6.7 (Hajdu and Larsson, 2006), whereas the same species thrives
557 in the Galician Rias at 15-18 °C and salinities > 35 (Velo-Suárez et al., 2008). Increased
558 numbers of *D. acuta* are usually related to years with positive temperature anomalies when
559 more persistent thermal stratification and deeper thermoclines are established (Díaz et al.,
560 2016).
561 Turbulence, a major physical forcing defining phytoplankton abundance and distribution
562 (Margalef, 1978), affects dinoflagellate population dynamics and physiology at the
563 microscale (Berdalet et al., 2017; Sullivan et al., 2003). There is a strong body of
564 information relating dinoflagellates blooms to low turbulence conditions (Glibert, 2016;
565 Margalef, 1978; Smayda and Reynolds, 2001). Díaz et al. (2019c) associated a decline in
566 the division rate of *D. acuminata* with increased turbulence combined with a rapid fall of
567 temperature (> 2 °C) during an upwelling event. Laboratory experiments show that *D.*
568 *acuta* is more sensitive to medium ($\varepsilon \approx 10^{-5}$ m^2s^{-3}) and high ($\varepsilon \approx 10^{-4}$ m^2s^{-3}) turbulent
569 mixing than *D. acuminata* (García-Portela et al., 2019).

570 The position of *D. acuta* on the OMI plane suggests that it avoided higher turbulence, while
571 *D. acuminata* endured more turbulent surface waters (Fig. 10B). Persistent high turbulence
572 ($\varepsilon \leq 10^{-5}$ m^2s^{-3}) on the second night may have caused a dispersion of *D. acuta*, generating a
573 window of opportunity for the more resistant *D. acuminata* and its prey (Fig. 4B, C). It is
574 important to note that the rise in *D. acuminata* numbers (from 16:00 h on February 27 to
575 4:00 h on February 28) coincided with the replacement of the inverse thermal stratification
576 (colder water at the surface) with an isothermal layer of warmer (18 °C) water in the upper
577 6 m. This rise in temperature may have been partly caused by insolation leading to
578 formation of a diurnal thermocline. Alternatively, the high density population of *D.*
579 *acuminata* may have been advected from other areas more favourable for growth. This
580 possibility is supported by the coincidence with increased turbulence, and by the fact that
581 high densities (> 5 x 10^3 cells L^{-1}) of *D. acuminata* were found two days before (February
582 24th) (data not shown) in surface waters 8 km south of the sampling station at the
583 confluence of Magdalena Sound and PF (Fig. 1C). Predominant southerly winds in summer
584 have been found to force unidirectional northward currents (Pinilla et al., 2020). These
585 observations are compatible with a possible wind-driven advection of the *D. acuminata*
586 population observed the second day, coinciding with flood tide.
587 The association of *D. acuminata* cell maxima with the diurnal thermocline was reported in
588 the Galician Rías (Velo-Suárez et al., 2008). In the same region, Pizarro et al (2008)
589 identified semidiurnal tides as a main factor underlying the diurnal variability of a *D. acuta*
590 bloom at a fixed station. Tides were also identified as a short time scale factor modulating
591 bloom formation of *Pseudo-nitzschia* species in an upwelling system (Díaz et al., 2014) and
592 *D. acuta* in Pitipalena, a nearby Chilean fjord (Díaz et al. 2011).
593

4.2. *Light and nutritional sources for* Dinophysis *species*

To date, all *Dinophysis* species in culture have been shown to be obligate mixotrophs that retain plastids (kleptoplastids) from their prey to perform photosynthesis (Hansen et al., 2013; Park et al., 2006; Riisgaard and Hansen, 2009). Nevertheless, each species has its own adaptations. Niche position on the OMI plane revealed that *D. acuta* tended to avoid surface waters (0 – 2m) where light intensity is high, while *D. acuminata* showed a preference for this parameter (Fig. 10B). García-Portela et al. (2018) found that *D. acuta* was more susceptible to photo-damage when exposed to high light intensities (370 – 650 µmol $m^{-2}s^{-1}$) in which *D. acuminata* can survive and grow. In addition, *D. acuta* was able to survive longer periods in the dark. These differences may explain the co-occurrence of *D. acuta* in subsurface layers (lower light intensity) with *D. acuminata* at the surface (high light) (García-Portela et al., 2018).

Field incubations with N^{15} labelled compounds in two upwelling areas showed *D. acuminata* preference for ammonia and organic nitrogen sources. Uptake rates of this species led the authors to classify it as a "high affinity strategist", adapted to grow with regenerated nitrogen sources in nutrient-poor environments (Seeyave et al., 2013; Seeyave et al., 2009). These preferences were confirmed in laboratory experiments (Hattenrath-Lehmann and Gobler 2015). García-Portela et al (2020) showed that neither *D. acuminata* nor *D. acuta* take up nitrate. A review of transcriptomic databases showed a paucity of nitrate transporter homologs in *D. acuminata*. Ammonia measurements were not made in the present study, but scarce (low vertical resolution) ammonia data from Chilean fjords shows concentrations in PF between 0.377 and 1.867 µmol L^{-1} (Gallardo-Carrasco, 2017; Prado-Fiedler, 2000). But nitrogen recycling rates are high and are overlooked in simple measurements of free ammonia. Culture experiments have shown that *Dinophysis* division

618 is triggered after ingestion of prey (Nielsen et al., 2012; Smith and Hansen, 2007).
619 Considering the high values of μ observed in this study and the healthy appearance of the
620 cells, including specimens swollen with digestive vacuoles (Fig. S2), it seems assured that
621 *Dinophysis* populations in PF were not food-limited.
622 *Mesodinium* species, mainly *M. rubrum*, are the only confirmed prey of *Dinophysis* and
623 source of their kleptoplastids in the field and in laboratory cultures. Likewise, cryptophytes
624 belonging to the *Teleaulax/Plagioselmis/Geminigera* (TPG) clade are the only known
625 group supporting growth of *Mesodinium*, which are also kleptoplastidic mixotrophs. These
626 trophic relations have been established in field populations when partial 23S rDNA
627 sequences of *Dinophysis* plastids match those of *Mesodinium* and its prey (e.g., *Teleaulax*
628 *amphioxeia*) (Rial et al. 2015). Recent observations in the Chilean fjords of *Dinophysis*
629 apparently feeding on ciliates other than *Mesodinium*, and the mismatch of their plastid
630 sequences with those of local *Mesodinium* fuelled the hypothesis of an alternative prey
631 (Díaz et al., 2020a). Furthermore, these authors demonstrated that *Dinophysis acuta, D.*
632 *caudata, D. tripos* and *D. subcircularis* from southern Chile had plastids of cryptophytes
633 belonging to clade V (*Rhinomonas/Rhodomonas/Storeatula*). That was the first report of
634 *Dinophysis* species with plastids from a cryptophyte clade other than the TPG clade. But
635 the ciliate prey (vector) transferring clade V cryptophytes plastids to *Dinophysis* was not
636 identified.
637 Analysis of the accompanying plastid-bearing ciliates in the present 48 h study did not
638 show any relationship between the daily vertical migration (DVM) of *D. acuta* and the
639 distribution of *Mesodinium* spp. (Fig. 4B and D), although *D. acuminata* and *Mesodinium*
640 populations coincided at the surface between 20:00 h and 00:00 h the second day when
641 both predator and potential prey reached their cell maxima (Fig. 4C, D). It is true that the

642 co-occurrence of ciliates other than *Mesodinium* species with *Dinophysis* does not provide
643 evidence of a trophic relationship; nevertheless, it gives a clue about ciliates species to be
644 tested in future studies to identify, with molecular tools, alternative prey in the Chilean
645 fjord's region.
646 In the Galician Rías, partial sequences of the plastids 23S rDNA of *Dinophysis* and
647 *Mesodinium* species were identical (Rial et al., 2015). During a 2 weeks cruise also in the
648 Rías, Díaz et al. (2019c) found that cell maxima of *D. acuminata* and its prey coincided at
649 noon when *Mesodinium* spp. migrated to the surface. *D. acuminata* formed a thin layer and
650 did not migrate, but with an angler´s strategy waited for its prey to pass by. Similar
651 observations were reported from the Baltic Sea by Sjöqvist and Lindholm (2011). Our
652 results illustrate an overlap of *D. acuminata* and *Mesodinium* at night (Fig. 4C and D).
653 Earlier studies concluded that *Dinophysis* and *Mesodinium* had distinct niches but co-
654 occurred in the same water masses and eventually met (González-Gil et al., 2010), thus
655 facilitating feeding of *D. acuminata* on its prey. These observations are compatible with the
656 mucilage secreted in cultures of *D. acuta* (Papiol et al., 2016) and *D. acuminata* , which
657 acts as a "mucus trap" and entangles the fast swimming ciliates. The OMI parameter values
658 show that environmental conditions during the 48 h study were common to both
659 *Mesodinium* species and *D. acuminata*. The two organisms share a high niche breadth (Fig.
660 10C), which allows them a wide distribution in the water column (Fig. 4D).
661 Other plastid-bearing ciliates described as potential prey co-occurred with *Dinophysis* in
662 the present study. The PERMANOVA analysis identified *Mesodinium* spp.,
663 *Pseudotontonia* sp. and *Strombidium* spp. as significant explanatory factors for the two
664 *Dinophysis* species (Table S3). However, the present information does not allow us to
665 attribute the *D. acuta* migrations or the distribution of *D. acuminata* to predation on one or

more of these potential prey. The question remains open pending new information on the plastid sequences of predators and potential prey. The OMI and PERMANOVA analysis results emphasize the importance of the different environmental variables considered here (i.e., abiotic: depth, temperature, salinity, turbulence, and PAR, and biotic: *Mesodinium* spp. and other potential prey). The PERMANOVA identified temperature, salinity, and PAR as significant factors to explain *Dinophysis* abundance and distribution (Table 2).

It is important to highlight that additional intrinsic factors or traits, such as cell morphology and swimming abilities may contribute to the response of each *Dinophysis* species to environmental factors. For example, *D. acuta* is more dorso-ventrally compressed, its volume three times larger and with a higher surface to volume ratio than the more rounded *D. acuminata* (García-Portela et al., 2018). These features make *D. acuta* more vulnerable to unstable conditions, such as those in the surface layers and facilitate the success of the more rounded *D. acuminata* in fresher and more illuminated surface waters subject to a wider range of temperature.

4.3. Dinophysis *in situ division rates, toxins, and behaviour*

4.3.1. In situ division rates

Data on i*n situ* division rates of *Dinophysis acuta* are scarce. When available, however, it allows to distinguish the contribution of intrinsic population growth from behavioural aggregation and wind driven advection (Farrell et al., 2014; Pizarro et al., 2008; Reguera et al., 2003). The estimate of μ (0.76 d^{-1}) during the second day of this study, exceeding one doubling per day, is the highest value ever reported in field populations of *D. acuta*. As in

688 earlier studies, the onset of light was the trigger for phased-cell division of *D. acuminata*;
689 *D. acuta* division started later, after sunrise (Fig. 7).
690 Reguera et al. (2003) suggested that the shape of the phase frequency curves show large
691 differences depending on the stage of *Dinophysis* population growth and the physiological
692 status of the cells. In general, division time (T_D, time between peaks of paired and recently
693 divided cells) was shorter, and the frequencies curve had a deeper slope in fit populations
694 with high division rates. Poor synchronization in division could be associated with late
695 phases of population growth (i.e., stationary phase), or be caused by increased cell numbers
696 due to physical accumulation or behaviour. The latter could have been the case of a
697 stationary phase population advected to the Galician Rías (Pizarro et al 2008). But T_D in the
698 present study was extremely short (less than 1 h) in both species, and with the exception of
699 the first cycle of *D. acuta*, frequency distributions looked like the overlapping of two
700 consecutive divisions (Fig. 7A, B). In any case, the high values of μ and the fact that the
701 maximal values of μ_{min} were observed at the same depth as the cell maximum (Fig. 8),
702 confirmed that active growth (higher in the case of *D. acuta*) contributed to the high
703 numbers observed for the two species during the 48 h study in PF. The exception was the
704 homogeneous vertical distribution of μ_{min} in *D. acuminata* the second day (28 Feb). It is
705 possible that this lack of layering was due to recent transport of cells.
706
707 *4.3.2. Toxin profiles*
708 The concentrations of OA and DTX-1 at 4m and 8m (Fig. 9 A, B) matched the vertical
709 distribution of *D. acuta*. Nevertheless, a small percentage of *D. acuminata* co-occurred with
710 *D. acuta* most of the time. The exception was in the samples from 0 m, where *D. acuta* and
711 diarrhetic toxins were hardly present. *D. acuminata* was the overwhelmingly dominant

712 species at 0 m with a cell maximum at this depth during a short time window, on the second
713 day. This coincided with a clear PTX-2 peak. Unambiguous identification of species-
714 specific toxin profiles in field populations of *Dinophysis* requires LC-MS analysis of
715 individually picked cells, as in Pizarro et al. (2013), or of unialgal cultures. So far, cultures
716 of *Dinophysis* have not been established in Chile, but analyses of picked cells of *D.* cf
717 *acuminata* from the north (Coquimbo) (Blanco et al., 2007) and south (Los Lagos) (Fux et
718 al. 2011; Blanco et al 2018) provinces have been made. In all these cases, PTX-2 was the
719 only toxin detected by LC-MS. PTX-2 was also the only toxin detected in plankton
720 concentrates from Reloncaví (Los Lagos) rich in *D. acuminata* (Alves-de-Souza et al.,
721 2014). More recently, PTX-2 was the only toxin reported in shellfish (*Tagelus dombeii*)
722 exposed to an intense spring bloom of *D. acuminata* on the central Chilean coast (Díaz et
723 al., 2020b). These results support the suspicion that the two diarrhetic toxins found during
724 the present study were both produced by *D. acuta.* and that at least in this region, *D. acuta*
725 is the main source of diarrhetic shellfish toxins. Since PTX-2 is not diarrheogenic by oral
726 administration, and pectenotoxins have been deregulated in some countries, these
727 differences in toxin profiles have an important impact on shellfish safety management.
728 Pending final confirmation, *D. acuta* is thus the species suspected of being the main cause
729 of DSP toxin (OA + DTXs) accumulation in shellfish in Southern Chile.
730

731 *4.3.3. Diurnal Vertical Migration*

732 *D. acuta* migrated (DVM) from 8 m during the day to 4 m at night, more clearly in the
733 first 24 h (Fig. 4B). This DVM had a similar short range but different pattern to that
734 observed during a bloom of *D. acuta* in Big Glory Bay (Steward Island, New Zealand),

735 with maxima at 15 m from 1:00 to 7:00, and at 10 m from 7:00 until the end of the study
736 at 22:00 (MacKenzie 1992). *D. acuminata* did not exhibit clear DVM, and cell maxima
737 were in the upper 2 m. There was no evidence of migration at all in the latter species in
738 some studies in the Galician Rías (Díaz et al., 2019c; Velo-Suárez et al., 2008). In
739 contrast, Villarino et al. (1995) described DVM of *D. acuminata*, from the surface
740 (1.25m) during the first hours of light, to ~ 10 m during the evening and night in Ría of
741 Vigo, also in the Galician Rías (NW Spain); this movement coincided with the DVM of
742 co-occurring dinoflagellates and of *Mesodinium*, and took place under extremely calm
743 conditions in thermally stratified waters in late summer (August). At the time, it was still
744 unknown that *Mesodinium* was a *Dinophysis* prey, and its migration was related to light
745 uptake during the day at the surface, and nutrient uptake at night in deeper waters. It is
746 well known that dinoflagellates can have distinct DVM patterns at different stages of
747 population growth or in response to the availability of resources, such as light, nutrients
748 and prey (Ross and Sharples, 2007). The position of the *D. acuta* maximum, coincident
749 with the vertical distribution of OA (117.6 ng OA mL^{-1}) (Fig. 9A), had no apparent
750 relation with tidal phase, but migration to upper layers at night could be related to prey
751 searching. In contrast, *D. acuminata* aggregations at the surface may have been using the
752 angler's strategy already described, to intercept *Mesodinium* cells during their morning
753 migration to the most illuminated surface layers (Díaz et al., 2019c; Sjöqvist and
754 Lindholm, 2011). A model from Yamazaki and Kamykowski (1991) predicts that cells
755 within a migrating population exposed to wind-induced vertical mixing do not migrate
756 uniformly but scatter within the mixed layer. A similar model might explain the even
757 vertical distribution of *D. acuminata* division rates at depth $(\mu_{min})_z$ the second day (Fig.
758 8).

5. Conclusions

This is the first time high vertical resolution hydrodynamic measurements including turbulence, have been made during intensive sampling of co-occurring blooms of *D. acuta*, *D. acuminata* and plastid bearing micro-ciliates in a stratified fjord system. Populations of the two *Dinophysis* species, in particular *D. acuta*, had very high division rates ($\mu > 0.6$ d^{-1}) and the depth of their respective cell density and division rate maxima coincided. Therefore, bloom densities resulted from a combination of intrinsic growth rate and physical factors which favoured niche differentiation of the two *Dinophysis* species. A realized niche approach (with an Outlying Mean Index analysis) applied to results from the 48 h study provided the opportunity to identify different environmental conditions defining these niches. The realized niche of *D. acuta*, was mainly defined by sub surface saltier waters with a strong influence of temperature, and avoidance of more turbulent and illuminated conditions at the surface. The realized niche of *D. acuminata* was characterized by estuarine surface waters with warmer temperatures and higher turbulence and light intensity. The apparent relationship between the ciliate *Mesodinium* and the distribution of *D. acuminata*, but not with *D. acuta*, is compatible with hypothesis on alternative plastid-retaining ciliate prey for *Dinophysis*. Cell maximum of *D. acuta* was associated with peaks of DSP toxins (OA + DTX-1) and PTX-2. In contrast, only PTX-2 was found in detectable amounts associated with a dense *D. acuminata* patch where this species represented > 96% of the total number of *Dinophysis*. These observations suggest (awaiting confirmation by picked cell analyses) that *D. acuta* is the main source of DSP toxins in Southern Chile, whereas *D. acuminata* appears related only to PTX-2. Field concentrations of *Dinophysis* may be over one order of magnitude higher than estimates from water column integrated hose samples collected in the official monitoring programme. Results from this study

783 improve current knowledge on conditions promoting blooms of two species of *Dinophysis*
784 with distinct impacts on aquaculture resources.
785
786 **Acknowledgements**
787 This work was funded by ANID-FONDECYT 11170682 from the National Agency of
788 Research and Development (ANID), Chile, and by projects REDES170101 and
789 REDI170575 from ANID International Cooperation Programme. C. F-P. was supported by
790 grant IN607A 2018/2 from the Axencia Galega de Innovación (Galicia, Spain); I. P-S. by
791 COPAS Sur-Austral AFB170006 and CIEP R20F002; F.B. by ANID-FONDECYT
792 3180307 and B. R by EU - Interreg Atlantic Area project PRIMROSE (EAPA_182/2016).
793 A. M. B. had a Ph.D student fellowship from Universidad de Los Lagos. We thank A. Bode
794 from IEO, Centro Oceanográfico de A Coruña, Spain, for valuable comments.
795
796 **References**
797 Álvarez, G., Uribe, E., Regueiro, J., Blanco, J., Fraga, S., 2016. *Gonyaulax taylorii*, a new
798 yessotoxins-producer dinoflagellate species from Chilean waters. Harmful Algae
799 58, 8-15.
800 Alves-de-Souza, C., Benevides, T.S., Santos, J.B., Von Dassow, P., Guillou, L., Menezes,
801 M., 2017. Does environmental heterogeneity explain temporal β diversity of small
802 eukaryotic phytoplankton? Example from a tropical eutrophic coastal lagoon. J.
803 Plankton Res. 39 (4), 698-714.
804 Alves-de-Souza, C., Iriarte, J.L., Mardones, J.I., 2019. Interannual variability of *Dinophysis*
805 *acuminata* and *Protoceratium reticulatum* in a Chilean Fjord: Insights from the
806 realized niche analysis. Toxins 11 (1), 19.

807 Alves-de-Souza, C., Varela, D., Contreras, C., de La Iglesia, P., Fernández, P., Hipp, B.,
808 Hernández, C., Riobó, P., Reguera, B., Franco, J.M., 2014. Seasonal variability of
809 *Dinophysis spp.* and *Protoceratium reticulatum* associated to lipophilic shellfish
810 toxins in a strongly stratified Chilean fjord. Deep-Sea Res. Pt. II. 101, 152-162.
811 Anderson, M.J., 2014. Permutational multivariate analysis of variance (PERMANOVA).
812 Wiley statsref: statistics reference online, 1-15.
813 Avaria, S., 2008. Phytoplankton in the austral Chilean channels and fjords. In: N. Silva &
814 S. Palma (eds). Progress in the oceanographic knowledge of Chilean interior waters,
815 from Puerto Montt to Cape Horn. Comité Oceanográfico Nacional - Pontificia
816 Universidad Católica de Valparaíso, Valparaíso, 89-92.
817 Berdalet, E., Montresor, M., Reguera, B., Roy, S., Yamazaki, H., Cembella, A., Raine, R.,
818 2017. Harmful algal blooms in fjords, coastal embayments, and stratified systems:
819 recent progress and future research. Oceanography 30 (1), 46-57.
820 Blanco, J., Álvarez, G., Rengel, J., Díaz, R., Mariño, C., Martín, H., Uribe, E., 2018.
821 Accumulation and biotransformation of *Dinophysis* toxins by the surf clam
822 *Mesodesma donacium*. Toxins 10 (8), 314.
823 Blanco, J., Álvarez, G., Uribe, E., 2007. Identification of pectenotoxins in plankton, filter
824 feeders, and isolated cells of *Dinophysis acuminata* with an atypical toxin profile,
825 from Chile. Toxicon 49 (5), 710-716.
826 Brun, P., Vogt, M., Payne, M.R., Gruber, N., O'Brien, C.J., Buitenhuis, E.T., Le Quéré, C.,
827 Leblanc, K., Luo, Y.W., 2015. Ecological niches of open ocean phytoplankton taxa.
828 Limnol. Oceanogr. 60 (3), 1020-1038.

Calvete, C., Sobarzo, M., 2011. Quantification of the surface brackish water layer and frontal zones in southern Chilean fjords between Boca del Guafo (43° 30′ S) and Estero Elefantes (46° 30′ S). Cont. Shelf Res. 31 (3-4), 162-171.

Carpenter, E.J., Chang, J., 1988. Species-specific phytoplankton growth rates via diel DNA synthesis cycles. 1. Concept of the method. Mar. Ecol. Prog. Ser. 43 (1), 105-111.

Cassis, D., Muñoz, P., Avaria, S., 2002. Variación temporal del fitoplancton entre 1993 y 1998 en una estación fija del seno Aysén, Chile (45º26'S 73º00'W). Rev. Biol. Mar. Oceanog. 37 (1), 43-65.

Colwell, R.K., Rangel, T.F., 2009. Hutchinson's duality: the once and future niche. Pro. Natl. Acad. Sci. 106 (Supplement 2), 19651-19658.

Díaz, P., Fernández-Pena, C., Pérez-Santos, I., Baldrich, A., Díaz, M., Rodríguez, F., 2020a. *Dinophysis* Ehrenberg (Dinophyceae) in Southern Chile harbours red cryptophyte plastids from *Rhodomonas/Storeatula* clade. Harmful Algae 99, 101907.

Díaz, P., Molinet, C., Cáceres, M.A., Valle-Levinson, A., 2011. Seasonal and intratidal distribution of *Dinophysis* spp. in a Chilean fjord. Harmful Algae 10 (2), 155-164.

Díaz, P.A., Álvarez, A., Varela, D., Pérez-Santos, I., Díaz, M., Molinet, C., Seguel, M., Aguilera-Belmonte, A., Guzmán, L., Uribe, E., Rengel, J., Hernández, C., Segura, C., Figueroa, R. I., 2019a. Impacts of harmful algal blooms on the aquaculture industry: Chile as a case study. Perspectives in Phycology 6 (1-2), 39-50.

Díaz, P.A., Álvarez, G., Seguel, M., Marín, A., Krock, B., 2020b. First detection of pectenotoxin-2 in shellfish associated with an intense spring bloom of *Dinophysis acuminata* on the central Chilean coast. Mar. Pollut. Bull. 158, 111414.

Díaz, P.A., Peréz-Santos, I., Álvarez, G., Garreaud, R., Pinilla, E., Díaz, M., Sandoval, A., Araya, M., Álvarez, F., Rengel, J., Montero, P., Pizarro, G., López, L., Iriarte, L., Igor, G., Reguera, B., 2021. Multiscale physical background to an exceptional harmful algal bloom of *Dinophysis acuta* in a fjord system. Sci. Total Environ. 773, 145621.

Díaz, P.A., Reguera, B., Moita, T., Bravo, I., Ruiz-Villarreal, M., Fraga, S., 2019b. Mesoscale dynamics and niche segregation of two *Dinophysis* species in Galician-Portuguese coastal waters. Toxins 11 (1), 37.

Díaz, P.A., Ruiz-Villarreal, M., Mouriño-Carballido, B., Fernández-Pena, C., Riobó, P., Reguera, B., 2019c. Fine scale physical-biological interactions during a shift from relaxation to upwelling with a focus on *Dinophysis acuminata* and its potential ciliate prey. Prog. Oceanogr. 175, 309-327.

Díaz, P.A., Ruiz-Villarreal, M., Pazos, Y., Moita, T., Reguera, B., 2016. Climate variability and *Dinophysis acuta* blooms in an upwelling system. Harmful Algae 53, 145-159.

Díaz, P.A., Ruiz-Villarreal, M., Velo-Suárez, L., Ramilo, I., Gentien, P., Lunven, M., Fernand, L., Raine, R., Reguera, B., 2014. Tidal and wind-event variability and the distribution of two groups of *Pseudo-nitzschia* species in an upwelling-influenced Ría. Deep-Sea Res. Pt. II. 101, 163-179.

Dolédec, S., Chessel, D., Gimaret-Carpentier, C., 2000. Niche separation in community analysis: a new method. Ecology 81 (10), 2914-2927.

Dray, S., Dufour, A.-B., 2007. The ade4 package: implementing the duality diagram for ecologists. J. Stat. Softw. 22 (4), 1-20.

874 Escalera, L., Reguera, B., Moita, T., Pazos, Y., Cerejo, M., Cabanas, J.M., Ruiz-Villarreal,
875 M., 2010. Bloom dynamics of *Dinophysis acuta* in an upwelling system: In situ
876 growth versus transport. Harmful Algae 9(3), 312-322.
877 Escalera, L., Reguera, B., Pazos, Y., Moroño, A., Cabanas, J., 2006. Are different species
878 of *Dinophysis* selected by climatological conditions? Afr. J. Mar. Sci. 28 (2), 283-
879 288.
880 EURLMB, 2015. EU Harmonised standard operating procedure for determination of
881 lipophilic marine biotoxins in mollucs by LC-MS/MS. Version 5, 1-33.
882 European Commission., 2019. Commission Implementing Regulation (EU) 2019/627 of 15
883 March 2019 laying down uniform practical arrangements for the performance of
884 official controls on products of animal origin intended for human consumption in
885 accordance with Regulation (EU) 2017/625 of the European Parliament and of the
886 Council and amending Commission Regulation (EC) No 2074/2005 as regards
887 official controls. Off. J. Eur. Union L131, 51.
888 Farrell, H., Velo-Suárez, L., Reguera, B., Raine, R., 2014. Phased cell division, specific
889 division rates and other biological observations of *Dinophysis* populations in sub-
890 surface layers off the south coast of Ireland. Deep-Sea Res. Pt. II: Topical Stud.
891 Oceanography 101, 249-254.
892 Fernández, R., Mamán, L., Jaén, D., Fuentes, L., Ocaña, M.A., Gordillo, M.M., 2019.
893 *Dinophysis* species and diarrhetic shellfish toxins: 20 years of monitoring program
894 in Andalusia, South of Spain. Toxins 11 (4), 189.
895 Fux, E., Smith, J.L., Tong, M., Guzmán, L., Anderson, D.M., 2011. Toxin profiles of five
896 geographical isolates of *Dinophysis* spp. from North and South America. Toxicon
897 57 (2), 275-287.

898 Gaillard, S., Le Goïc, N., Malo, F., Boulais, M., Fabioux, C., Zaccagnini, L., Carpentier, L.,
899 Sibat, M., Réveillon, D., Séchet, V., 2020. Cultures of *Dinophysis sacculus*, *D.*
900 *acuminata* and pectenotoxin 2 affect gametes and fertilization success of the Pacific
901 oyster, *Crassostrea gigas*. Environ. Pollut. 265, 114840.
902 Gallardo-Carrasco, M.P., 2017. ¿Existe una relación entre biomasa fitoplanctónica y
903 concentración de amonio en fiordos patagónicos? Ing. degree Thesis. Universidad
904 Austral de Chile, Puerto Montt-Chile.
905 García-Portela, M., Reguera, B., Ribera d'Alcalà, M.R., Rodríguez, F., Montresor, M.,
906 2019. Effects of small-scale turbulence on two species of *Dinophysis*. Harmful
907 Algae 89, 101654.
908 García-Portela, M., Reguera, B., Gago, J., Gac, M.L., Rodríguez, F., 2020. Uptake of
909 Inorganic and Organic Nitrogen Sources by *Dinophysis acuminata* and *D. acuta*.
910 Microorganisms 8 (2), 187.
911 García-Portela, M., Riobó, P., Reguera, B., Garrido, J.L., Blanco, J., Rodríguez, F., 2018.
912 Comparative ecophysiology of *Dinophysis acuminata* and *D. acuta* (Dinophyceae,
913 Dinophysiales): effect of light intensity and quality on growth, cellular toxin
914 content, and photosynthesis. J. Phycol. 54 (6), 899-917.
915 García, C., González, V., Cornejo, C., Palma-Fleming, H., Lagos, N., 2004. First evidence
916 of Dinophysistoxin-1 ester and carcinogenic polycyclic aromatic hydrocarbons in
917 smoked bivalves collected in the Patagonia fjords. Toxicon 43 (2), 121-131.
918 GEOHAB, 2008. Global Ecology and Oceanography of Harmful Algal Blooms, GEOHAB
919 Core Research Project: HABs in Stratified Systems. P. Gentien, B. Reguera, H.
920 Yamazaki, L. Fernand, E. Berdalet, and R. Raine (Eds.). IOC and SCOR, Paris,
921 France, and Newark, Delaware, USA. 59pp.

922 GEOHAB, 2011. GEOHAB Modelling: A Workshop Report. D.J. McGillicuddy, Jr., P.M.
923 Glibert, E. Berdalet, C. Edwards, P. Franks, and O. Ross (eds). IOC and SCOR,
924 Paris and Newark, Delaware, 85pp.
925 Gestal-Otero, J.J., 2014. Epidemiology of marine toxins, In: Botana, L.M. (Ed.), Seafood
926 and Freshwater Toxins: Pharmacology, Physiology, and Detection, 3rd ed. CRC
927 Press, Taylor and Francis Group, Boca Ratón, FL, USA. pp. 123-195.
928 Glibert, P.M., 2016. Margalef revisited: a new phytoplankton mandala incorporating twelve
929 dimensions, including nutritional physiology. Harmful Algae 55, 25-30.
930 González-Gil, S., Velo-Suárez, L., Gentien, P., Ramilo, I., Reguera, B., 2010.
931 Phytoplankton assemblages and characterization of a *Dinophysis acuminata*
932 population during an upwelling–downwelling cycle. Aquat. Microb. Ecol. 58 (3),
933 273-286.
934 Grasshoff, K., Ehrhardt, M., Kremling, K., 1983. Methods of seawater analysis. Verlag
935 Chemie Weinhein, New York, USA.
936 Grüner, N., Gebühr, C., Boersma, M., Feudel, U., Wiltshire, K.H., Freund, J.A., 2011.
937 Reconstructing the realized niche of phytoplankton species from environmental
938 data: fitness versus abundance approach. Limnol. Oceanogr. Meth. 9 (10), 432-442.
939 Hajdu, S., Larsson, U., 2006. Life-cycle stages of *Dinophysis acuminata* (Dinophyceae) in
940 the Baltic Sea. Afr. J. Mar. Sci. 28 (2), 289-293.
941 Hansen, P.J., Nielsen, L.T., Johnson, M., Berge, T., Flynn, K.J., 2013. Acquired
942 phototrophy in *Mesodinium* and *Dinophysis* – A review of cellular organization,
943 prey selectivity, nutrient uptake and bioenergetics. Harmful Algae 28, 126-139.

Hattenrath-Lehmann, T., Gobler, C.J., 2015. The contribution of inorganic and organic nutrients to the growth of a North American isolate of the mixotrophic dinoflagellate, *Dinophysis acuminata*. Limmol. Oceanogr. 60, 1588–1603.

Hernández-Fariñas, T., Bacher, C., Soudant, D., Belin, C., Barillé, L., 2015. Assessing phytoplankton realized niches using a French national phytoplankton monitoring network. Estuar. Coast. Shelf Sci. 159, 15-27.

Holt, R.D., 2009. Bringing the Hutchinsonian niche into the 21st century: ecological and evolutionary perspectives. Proc. Natl. Acad. Sci. USA. 106 (Supplement 2), 19659-19665.

Hutchinson, G., 1957. Concluding remarks. Cold Spring Harbor Symposia on Quantitative biology. 22 (2), 415 - 427.

Irwin, A.J., Nelles, A.M., Finkel, Z.V., 2012. Phytoplankton niches estimated from field data. Limnol. Oceanogr. 57 (3), 787-797.

Karasiewicz, S., Breton, E., Lefebvre, A., Fariñas, T.H., Lefebvre, S., 2018. Realized niche analysis of phytoplankton communities involving HAB: *Phaeocystis* spp. as a case study. Harmful Algae 72, 1-13.

Karasiewicz, S., Chapelle, A., Bacher, C., Soudant, D., 2020. Harmful algae niche responses to environmental and community variation along the French coast. Harmful Algae 93, 101785.

Karasiewicz, S., Dolédec, S., Lefebvre, S., 2017. Within outlying mean indexes: refining the OMI analysis for the realized niche decomposition. PeerJ 5, 3364.

Kattner, G., Becker, H., 1991. Nutrients and organic nitrogenous compounds in the marginal ice zone of the Fram Strait. J. Mar. Syst. 2, 385-394.

967 Kim, M., Kim, S., Yih, W., Park, M.G., 2012. The marine dinoflagellate genus *Dinophysis*
968 can retain plastids of multiple algal origins at the same time. Harmful Algae 13,
969 105-111.
970 Kim, S., Kang, Y.G., Kim, H.S., Yih, W., Coats, D.W., Park, M.G., 2008. Growth and
971 grazing responses of the mixotrophic dinoflagellate *Dinophysis acuminata* as
972 functions of light intensity and prey concentration. Aquat. Microb. Ecol. 51 (3),
973 301-310.
974 Litchman, E., Edwards, K.F., Klausmeier, C.A., Thomas, M.K., 2012. Phytoplankton
975 niches, traits and eco-evolutionary responses to global environmental change. Mar.
976 Ecol. Prog. Ser. 470, 235-248.
977 Lovegrove, T., 1960. An improved form of sedimentation apparatus for use with an
978 inverted microscope. ICES J. Mar. Sci. 25 (3), 279-284.
979 Luketina, D.A., Imberger, J., 2001. Determining turbulent kinetic energy dissipation from
980 Batchelor curve fitting. J. Atmos. Ocean. Tech. 18 (1), 100-113.
981 MacKenzie, L., 1992. Does Dinophysis (Dinophyceae) have a sexual life cycle? J. Phycol.
982 28(3), 399-406.
983 Maestrini, S.Y., 1998. Bloom dynamics and ecophysiology of *Dinophysis* spp., In: D.M.
984 Anderson, A.D. Cembella, and G.M. Hallegraeff (Ed.), Physiological Ecology of
985 Harmful Algal Blooms. NATO ASI Series, Series G, Ecological Science, Springer-
986 Verlag, Berlin, Heidelberg, New York, pp. 243-266.
987 Margalef, R., 1978. Life-forms of phytoplankton as survival alternatives in an unstable
988 environment. Oceanol. Acta 1 (4), 493-509.

McDuff, R., Chisholm, S., 1982. The calculation of in situ growth rates of phytoplankton populations from fractions of cells undergoing mitosis: a clarification 1. Limnol. Oceanogr. 27 (4), 783-788.

Moita, M., Sobrinho-Gonçalves, L., Oliveira, P., Palma, S., Falcão, M., 2006. A bloom of *Dinophysis acuta* in a thin layer off North-West Portugal. Afr. J. Mar. Sci. 28 (2), 265-269.

Munday, R., 2014. Toxicology of seafood toxins: a critical review, In: M.L. Botana (Ed.), Seafood and Freshwater Toxins, Pharmacology, Physiology and Detection. CRC Press, Boca Raton, FL, USA, pp. 197–290.

Muñoz, P., 1992. Presencia de dinoflagelados tóxicos del género *Dinophysis* en el seno de Aysén, Chile. Rev. Biol. Mar. Valparaiso 27, 187-212.

Nielsen, L.T., Krock, B., Hansen, P.J., 2012. Effects of light and food availability on toxin production, growth and photosynthesis in *Dinophysis acuminata*. Mar. Ecol. Prog. Ser. 471, 37-50.

Oksanen, J., Blanchet, G., Friendly, M., Kindt, R., Legendre, P., McGlinn, D., Minchin, P., O'Hara, R., Simpson, G., Solymos, P., Henry, M., Stevens, H., Szoecs, E., Wagner, H., 2018. Vegan: community ecology package. R package version 2(6).

Pagel, J., Schurr, F.M., 2012. Forecasting species ranges by statistical estimation of ecological niches and spatial population dynamics. Global Ecol. Biogeogr. 21 (2), 293-304.

Palma, A.S, Vilarihno, M.G, Moita, M.T., 1998. Interannual trends in the longshore distribution of *Dinophysis* off the Portuguese coast. In: Reguera, B., Blanco, J., Fernández, M.L., Wyatt, T (eds) Harmful Algae. Xunta de Galicia and

Intergovernmental Oceanographic Commission of UNESCO, Santiago de Compostela, pp. 124–127.

Papiol, G.G., Beuzenberg, V., Selwood, A.I., MacKenzie, L., Packer, M.A., 2016. The use of a mucus trap by *Dinophysis acuta* for the capture of *Mesodinium rubrum* prey under culture conditions. Harmful Algae 58, 1-7.

Park, M.G., Kim, S., Kim, H.S., Myung, G., Kang, Y.G., Yih, W., 2006. First successful culture of the marine dinoflagellate *Dinophysis acuminata*. Aquat. Microb. Ecol. 45 (2), 101-106.

Paterson, R.F., McNeill, S., Mitchell, E., Adams, T., Swan, S.C., Clarke, D., Miller, P.I., Bresnan, E., Davidson, K., 2017. Environmental control of harmful dinoflagellates and diatoms in a fjordic system. Harmful algae 69, 1-17.

Pérez-Santos, I., Garcés-Vargas, J., Schneider, W., Ross, L., Parra, S., Valle-Levinson, A., 2014. Double-diffusive layering and mixing in Patagonian fjords. Prog. Oceanogr. 129, 35-49.

Pickard, G., 1971. Some physical oceanographic features of inlets of Chile. J. Fish. Board Can. 28 (8), 1077-1106.

Pinilla, E., Castillo, M., Pérez-Santos, I., Venegas, O., Valle-Levinson, A., 2020. Water age variability in a Patagonian fjord. J. Mar. Syst. 103376.

Pizarro, G., Alarcón, C., Franco, J., Palma, M., Escalera, L., Reguera, B., Vidal, G., Guzmán, L., 2011. Spatial distribution of *Dinophysis* spp. and detection in water of DSP toxins through diaion resins (summer 2006, Los Lagos Region, Chile). Ciencia y Tecnología del Mar 34 (1/2), 31-48.

1034 Pizarro, G., Escalera, L., González-Gil, S., Franco, J.M., Reguera, B., 2008. Growth,
1035 behaviour and cell toxin quota of *Dinophysis acuta* during a daily cycle. Mar. Ecol.
1036 Prog. Ser. 353, 89-105.
1037 Pizarro, G., Moroño, Á., Paz, B., Franco, J., Pazos, Y., Reguera, B., 2013. Evaluation of
1038 passive samplers as a monitoring tool for early warning of *Dinophysis* toxins in
1039 shellfish. Mar. Drugs 11 (10), 3823-3845.
1040 Pizarro, G., Paz, B., Alarcón, C., Toro, C., Frangópulos, M., Salgado, P., Olave, C.,
1041 Zamora, C., Pacheco, H., Guzmán, L., 2018. Winter distribution of toxic,
1042 potentially toxic phytoplankton, and shellfish toxins in fjords and channels of the
1043 Aysén region, Chile. Lat. Am. J. Aquat. Res. 46 (1), 120-139.
1044 Prado-Fiedler, R., 2000. Spring distribution of ammonium in fjords and inlets between
1045 Puerto Montt and laguna San Rafael. Ciencia y Tecnología del Mar 23, 15-24.
1046 R Core Team, 2019. R: A language environment for statistical computing. R Foundation
1047 for Statistical Computing, Vienna, Austria. URL https://www.R-project.org/.
1048 Raine, R., Berdalet, E., Yamazaki, H., Jenkinson, I., Reguera, B., 2018. Key questions and
1049 recent research advances on Harmful Algal Blooms in stratified systems. In:
1050 Glibert, P., Berdalet, E., Burford, M., Pitcher, G., Zhou, M. (eds) Global Ecology
1051 and Oceanography of Harmful Algal Blooms. Ecological Studies, 232: 165-186.
1052 Regueiro, J., Rossignoli, A.E., Álvarez, G., Blanco, J., 2011. Automated on-line solid-
1053 phase extraction coupled to liquid chromatography–tandem mass spectrometry for
1054 determination of lipophilic marine toxins in shellfish. Food Chem. 129 (2), 533-540.
1055 Reguera, B., Bravo, I., Mariño, J., Campos-Loriz, M.J., Fraga, S., Carbonell, A., 1993.
1056 Trends in the occurrence of *Dinophysis* spp. in Galician coastal waters. In:

Smayda,T.J., Shimizu, Y. (Eds.), Toxic Phytoplankton Blooms in the Sea. Elsevier, Amsterdam, pp. 559–564.

Reguera, B., Garcés, E., Pazos, Y., Bravo, I., Ramilo, I., González-Gil, S., 2003. Cell cycle patterns and estimates of in situ division rates of dinoflagellates of the genus *Dinophysis* by a postmitotic index. Mar. Ecol. Prog. Ser. 249, 117-131.

Reguera, B., Riobó, P., Rodríguez, F., Díaz, P., Pizarro, G., Paz, B., Franco, J., Blanco, J., 2014. *Dinophysis* toxins: causative organisms, distribution and fate in shellfish. Mar. Drugs 12 (1), 394-461.

Reguera, B., Velo-Suárez, L., Raine, R., Park, M.G., 2012. Harmful *Dinophysis* species: A review. Harmful Algae 14, 87-106.

Rial, P., Laza-Martínez, A., Reguera, B., Raho, N., Rodríguez, F., 2015. Origin of cryptophyte plastids in *Dinophysis* from Galician waters: results from field and culture experiments. Aquat. Microb. Ecol. 76 (2), 163-174.

Riisgaard, K., Hansen, P.J., 2009. Role of food uptake for photosynthesis, growth and survival of the mixotrophic dinoflagellate *Dinophysis acuminata*. Mar. Ecol. Prog. Ser. 381, 51-62.

Ross, O.N., Sharples, J., 2007. Phytoplankton motility and the competition for nutrients in the thermocline. Mar. Ecol. Prog. Ser. 347, 21-38.

Rountos, K.J., Kim, J.J., Hattenrath-Lehmann, T.K., Gobler, C.J., 2019. Effects of the harmful algae, *Alexandrium catenella* and *Dinophysis acuminata*, on the survival, growth, and swimming activity of early life stages of forage fish. Mar. Environ. Res. 148, 46-56.

Roy, S., Montresor, M., Cembella, A., 2018. Key questions and recent research advances on Harmful Algal Blooms in fjords and coastal embayments. In: Glibert, P.,

Berdalet, E., Burford, M., Pitcher, G., Zhou, M. (eds) Global Ecology and Oceanography of Harmful Algal Blooms. Ecological Studies, 232: 187-203.

Sauter, T., 2020. Revisiting extreme precipitation amounts over southern South America and implications for the Patagonian Icefields. Hydrol. Earth Syst. Sci. 24, 203-2016.

Schlitzer, R., 2019. Ocean Data View, https://odv.awi.de.

Schneider, W., Pérez-Santos, I., Ross, L., Bravo, L., Seguel, R., Hernández, F., 2014. On the hydrography of Puyuhuapi Channel, Chilean Patagonia. Prog. Oceanogr. 129, 8-18.

Seeyave, S., Probyn, T., Álvarez-Salgado, X., Figueiras, F., Purdie, D., Barton, E., Lucas, M., 2013. Nitrogen uptake of phytoplankton assemblages under contrasting upwelling and downwelling conditions: The Ría de Vigo, NW Iberia. Estuar. Coast. Shelf Sci. 124, 1-12.

Seeyave, S., Probyn, T., Pitcher, G., Lucas, M., Purdie, D., 2009. Nitrogen nutrition in assemblages dominated by *Pseudo-nitzschia* spp., *Alexandrium catenella* and *Dinophysis acuminata* off the west coast of South Africa. Mar. Ecol. Prog. Ser. 379, 91-107.

Seguel, M., Tocornal, M.A., Sfeir, A., 2005. Floraciones algales nocivas en los canales y fiordos del sur de Chile. Ciencia y Tecnología del Mar 28 (2), 5-13.

Sievers, H., Silva, N., 2008. Water masses and circulation in austral Chilean channels and fjords. In: N. Silva & S. Palma (eds). Progress in the oceanographic knowledge of Chilean interior waters, from Puerto Montt to Cape Horn. Comité Oceanográfico Nacional - Pontificia Universidad Católica de Valparaíso, Valparaíso, 53-58.

1103 Silva, N., Calvete, C., 2002. Physical and chemical oceanographic features of southern
1104 Chilean inlets between Penas Gulf and Magellan Strait (Cimar-Fiordos 2 cruise).
1105 Ciencia y Tecnología del Mar 25, 23-28.
1106 Sjöqvist, C., Lindholm, T., 2011. Natural co-occurrence of *Dinophysis acuminata*
1107 (Dinoflagellata) and *Mesodinium rubrum* (Ciliophora) in thin layers in a coastal
1108 inlet. J. Eukaryot. Microbiol. 58 (4), 365-372.
1109 Smayda, T.J., 2002. Adaptive ecology, growth strategies and the global bloom expansion of
1110 dinoflagellates. J. Oceanogr. 58 (2), 281-294.
1111 Smayda, T.J., Reynolds, C.S., 2001. Community assembly in marine phytoplankton:
1112 application of recent models to harmful dinoflagellate blooms. J. Plankton Res. 23
1113 (5), 447-461.
1114 Smith, M., Hansen, P.J., 2007. Interaction between *Mesodinium rubrum* and its prey:
1115 importance of prey concentration, irradiance and pH. Mar. Ecol. Prog. Ser. 338, 61-
1116 70.
1117 Stoecker, D.K., Johnson, M.D., de Vargas, C., Not, F., 2009. Acquired phototrophy in
1118 aquatic protists. Aquat. Microb. Ecol. 57 (3), 279-310.
1119 Sullivan, J.M., Swift, E., Donaghay, P.L., Rines, J.E., 2003. Small-scale turbulence affects
1120 the division rate and morphology of two red-tide dinoflagellates. Harmful Algae 2
1121 (3), 183-199.
1122 Sutani, D., Utsumi, M., Kato, Y., Sugiura, N., 2014. Estimation of the changes in
1123 phytoplankton community composition in a volcanic acidotrophic Lake,
1124 Inawashiro, Japan. Jpn. J. Water Treat. Biol. 50 (2), 53-69.

Swan, S.C., Turner, A.D., Bresnan, E., Whyte, C., Paterson, R.F., McNeill, S., Mitchell, E., Davidson, K., 2018. *Dinophysis acuta* in Scottish coastal waters and its influence on Diarrhetic Shellfish Toxin profiles. Toxins 10 (10), 399.

ter Braak, C.J., Verdonschot, P.F., 1995. Canonical correspondence analysis and related multivariate methods in aquatic ecology. Aquat. Sci. 57 (3), 255-289.

Uribe, J.C., García, C., Rivas, M., Lagos, N., 2001. First report diarrheic shellfish toxins in magellanic fiords, southern Chile. J. Shellfish Res. 20, 69-74.

Utermöhl, H., 1958. Zur vervollkommnung der quantitativen Phytoplankton-Methodik: Mitt. Int. Vee. Ther. Angew. Limnol. 9: 1-38.

Velo-Suárez, L., González-Gil, S., Gentien, P., Lunven, M., Bechemin, C., Fernand, L., Raine, R., Reguera, B., 2008. Thin layers of *Pseudo-nitzschia* spp. and the fate of *Dinophysis acuminata* during an upwelling-downwelling cycle in a Galician Ría. Limnol. Oceanogr. 53 (5), 1816-1834.

Velo-Suárez, L., Reguera, B., Garcés, E., Wyatt, T., 2009. Vertical distribution of division rates in coastal dinoflagellate *Dinophysis* spp. populations: implications for modelling. Mar. Ecol. Prog. Ser. 385, 87-96.

Villarino, M., Figueiras, F., Jones, K., Álvarez-Salgado, X.A., Richard, J., Edwards, A., 1995. Evidence of in situ diel vertical migration of a red-tide microplankton species in Ria de Vigo (NW Spain). Mar. Biol. 123 (3), 607-617.

Yamazaki, H., Kamykowski, D., 1991. The vertical trajectories of motile phytoplankton in a wind-mixed water column. Deep-Sea Res. 38 (2), 219-241.

Yasumoto, T., Oshima, Y., Sugawara, W., Fukuyo, Y., Oguri, H., Igarashi, T., Fujita, N., 1980. Identification of *Dinophysis fortii* as the causative organism of diarrhetic shellfish poisoning. Bull. Jpn. Soc. Sci. Fish. 46(11), 1405-1411.

Table 1. Niche parameters estimated with the Outlying Mean Index (OMI) analysis for *Dinophysis acuta*, *D. acuminata* and their potential prey (microplanktonic ciliates) at a fixed sampling station in Puyuhuapi Fjord during the 48 h study (February 26 – 28, 2019). Niche parameters are given as absolute values for each species. Inertia (total variability), OMI (marginality), Tol (Tolerance), Rtol (Residual Tolerance). *P*-values were calculated with 10,000 random permutations that yielded a higher value than the observed marginality (OMI). Bold values were significant ($p < 0.05$).

Species	Code	Inertia	OMI	Tol	Rtol	*p*-value
Dinophysis acuta	*Dacuta*	4.13	0.65	1.49	2.00	**<0.01**
Dinophysis acuminata	*Dacuminata*	6.33	1.83	1.90	2.61	**<0.01**
Mesodinium spp.	*Meso*	5.41	0.10	3.11	2.19	**<0.01**
Leegaardiella sp.	*Leeg*	4.33	0.01	1.46	2.85	**<0.01**
Paratontonia spp.	*Para*	7.74	2.02	2.88	2.84	0.84
Strombidium spp.	*Strom*	5.81	0.49	2.97	2.36	**<0.01**
Pseudotontonia sp.	*Pse*	4.00	0.36	1.63	2.02	**<0.01**
Laboea sp.	*Labo*	4.68	0.91	1.86	1.91	**<0.01**
Lohmanniella sp.	*Loh*	4.63	0.16	2.21	2.27	**<0.01**
Cyrtostrombidium sp.	*Cyr*	1.88	0.25	0.12	1.52	0.29

Table 2. PERMANOVA analysis based on Euclidean method with the environmental variables explaining the cell densities of *D. acuta* and *D. acuminata* at a fixed sampling station in Puyuhuapi Fjord during the 48 h study (February 26 – 28, 2019). *P*-values were calculated with 10,000 random permutations. Bold values were significant ($p < 0.05$).

Predictive variables	Df	SS	R^2	Pseudo -F	*Pr >F*
Depth	1	5.44	0.00215	0.7444	0.4635
Temperature	1	313.87	0.12447	42.9327	**<0.05**
Salinity	1	323.26	0.12819	44.2176	**<0.05**
PAR	1	38.30	0.01518	5.2389	**<0.05**
Turbulence	1	18.27	0.00724	2.4992	0.0851
Residuals	186	1359.78	0.53926		
Total	191	2521.57	1.00000		

Figures

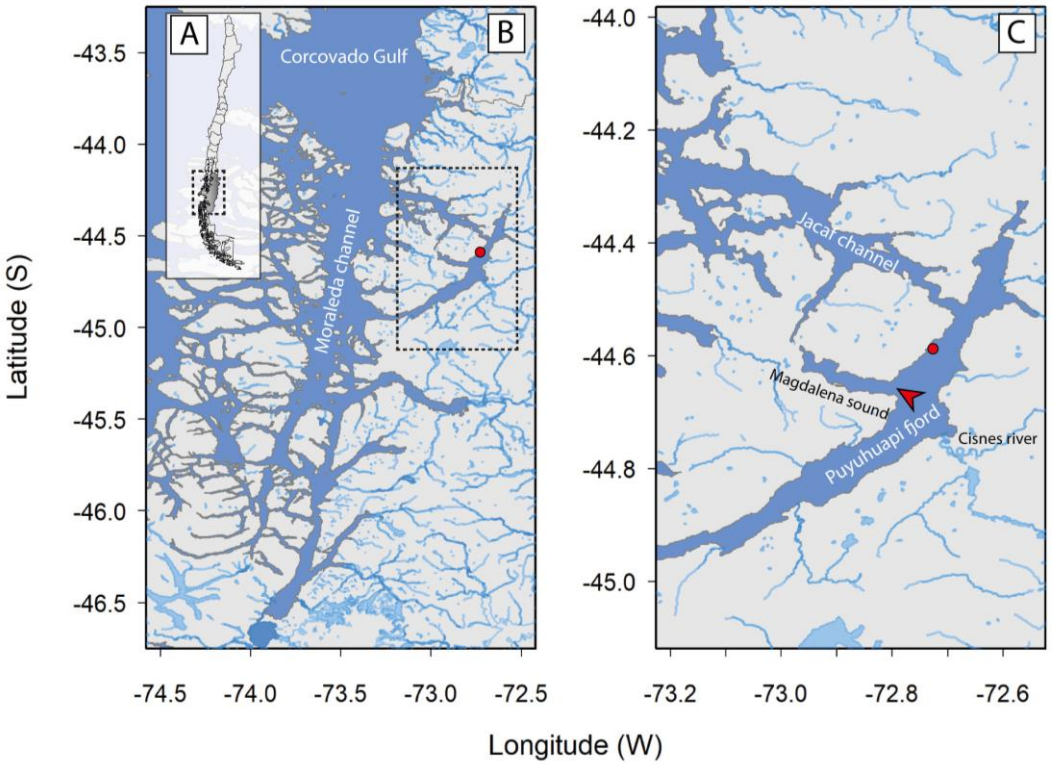

Figure 1. Map of the study area showing (A) Chile (the box delimits the Aysén region); (B) Aysén Region, Chilean Patagonia and its channels and fjords (the box delimits Puyuhuapi fjord); (C) Puyuhuapi Fjord and its main connections with the open sea, and freshwater

1174 sources. The red circle indicates the fixed sampling station for the 48 h study and the red
1175 arrow, the confluence zone between Magdalena Sound and Puyuhuapi Fjord.

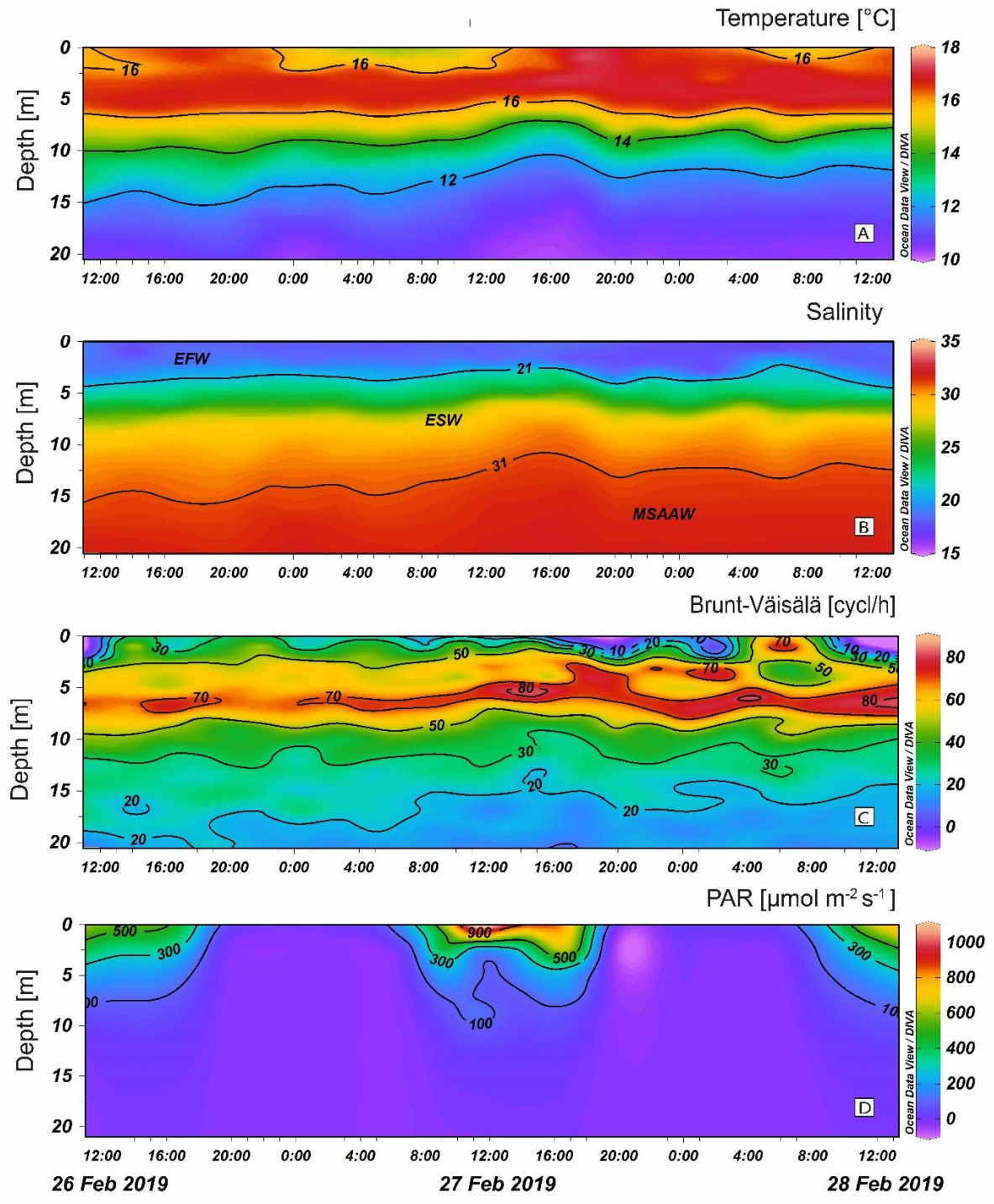

1176

Figure 2. Vertical distribution of (A) temperature (°C); (B) salinity; (C) Brünt-Väisälä frequency and (D) Photosynthetically Active Radiation (PAR) from measurements obtained every 2 h during 48 h at the fixed station with a Sea-Bird SBE-19 Conductivity - Temperature - Depth (CTD) probe cast from the surface to 50 m depth (A-C); and a Photosynthetically Active Radiation (PAR) sensor (D). Acronyms for water layers in Puyuhuapi Fjord, classified according to Pérez-Santos *et al.* (2019), stand for: EFW = Estuarine Fresh Water; ESW = Estuarine Salty Water; MSAAW = Modified Subantarctic water).

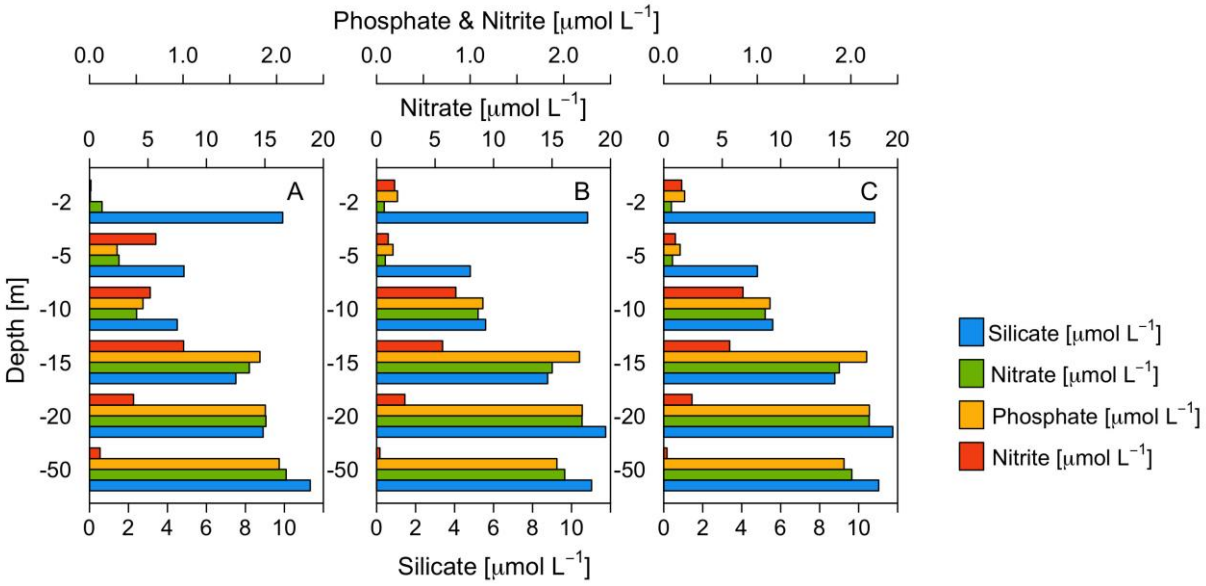

Figure 3. Vertical profiles of dissolved nutrients (silicate, nitrate, nitrite, and phosphate) at the fixed sampling station on: (A) 27 February; (B) 28 February and (C) 29 February 2019 at 12:00 h during the 48 h study.

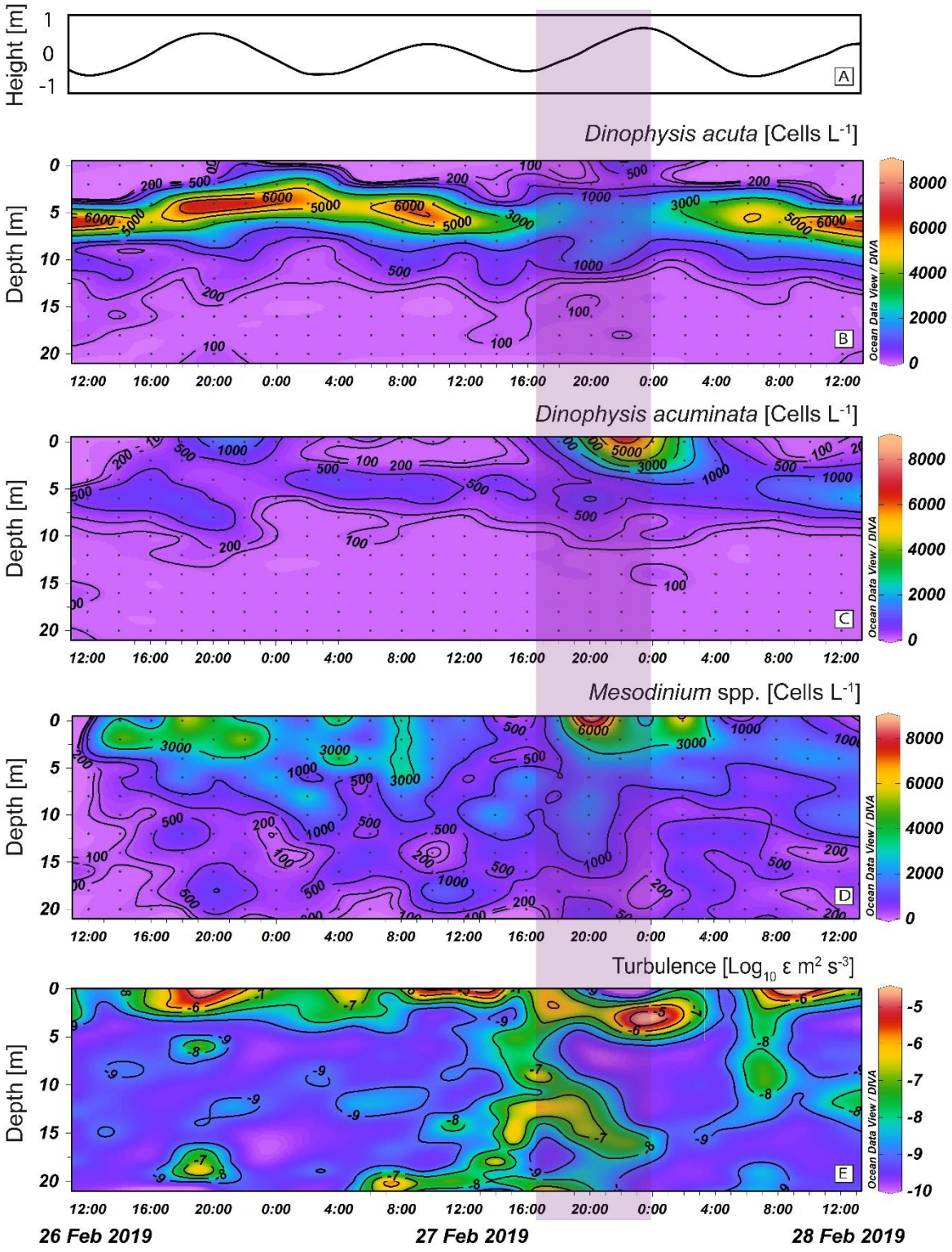

Figure 4. Vertical distribution of (A) Tidal amplitude; cell densities of (B) *Dinophysis acuta*; (C) *Dinophysis acuminata*; (D) *Mesodinium* spp.; (E) Turbulent kinetic energy

dissipation rate (ε) derived from the microstructure profiler deployed at the fixed station during the 48 h study (February 26 – 28, 2019). Shaded area indicates the hours of incoming tides and increased turbulence during the second day.

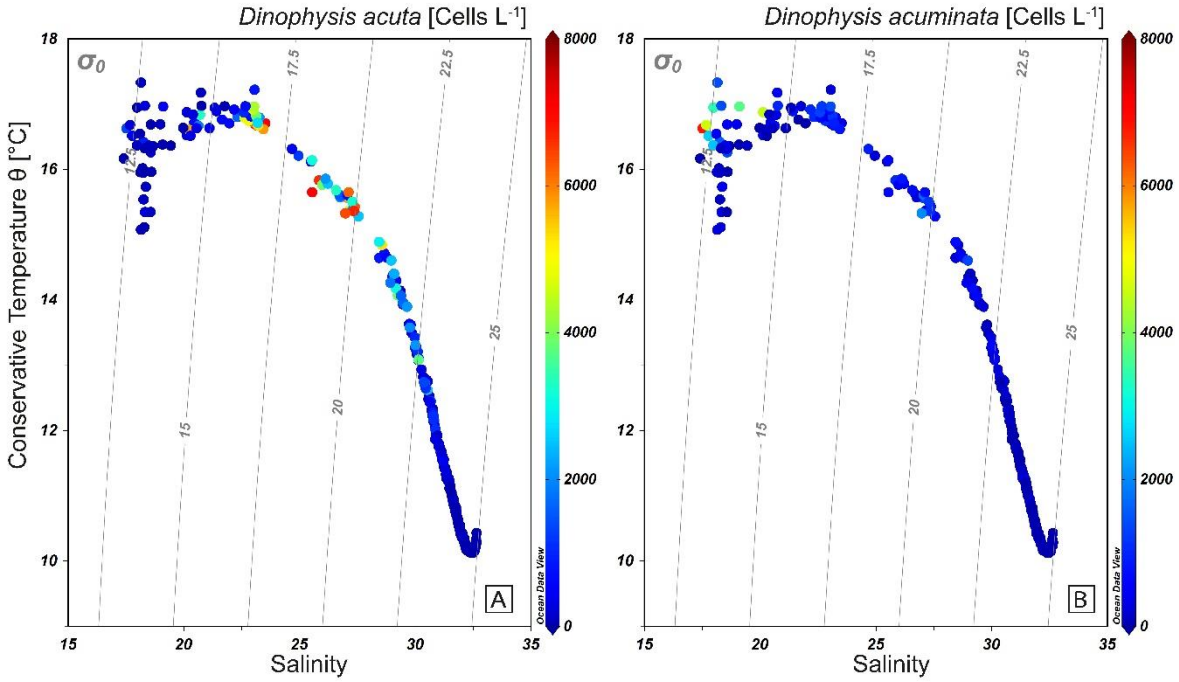

Figure 5. Cell densities of *D. acuta* (A) and *D. acuminata* (B) plotted over TS diagrams. Data from the fixed sampling station during the 48 h study (February 26 - 28, 2019). Gray contour lines represent isopycnals.

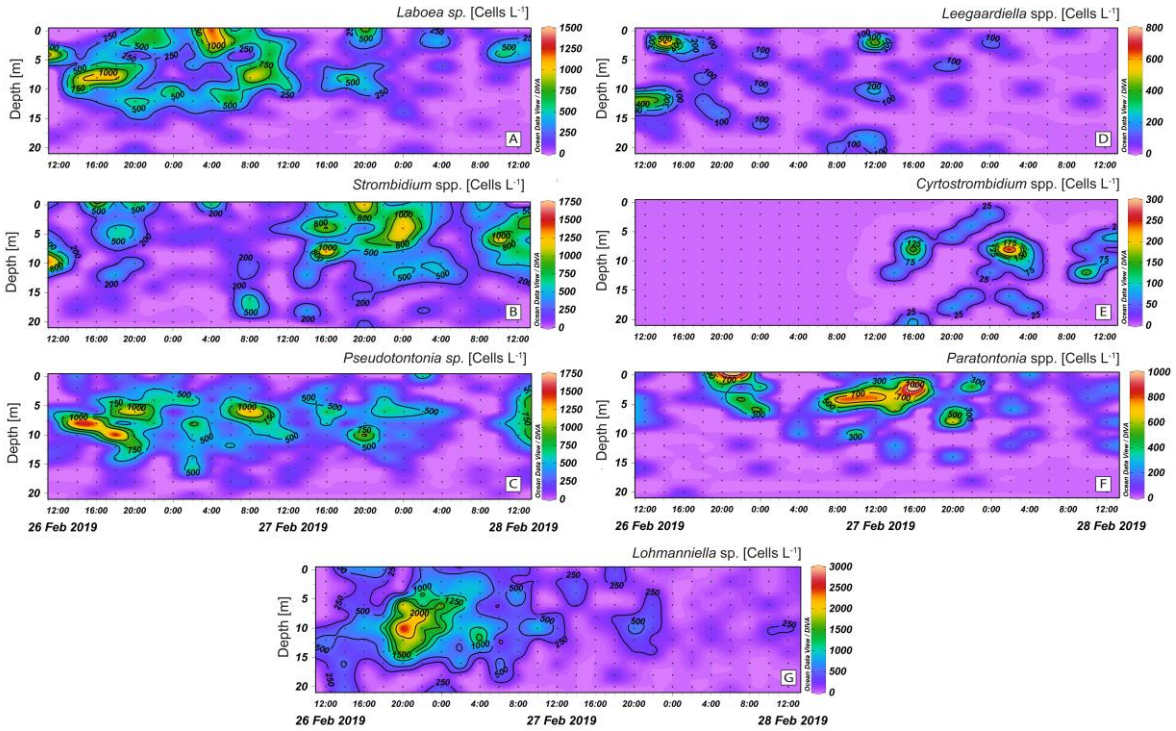

Figure 6. Vertical distribution of potential plastid-bearing micro-ciliate prey for *Dinophysis* species: (A) *Laboea* sp.; (B) *Strombidium* spp.; (C) *Pseudotontonia* sp.; (D) *Leegaardiella* spp.; (E) *Cyrtostrombidium* sp.; (F) *Paratontonia* spp.; (G) *Lohmanniella* sp. at the fixed sampling station during the 48 h study (February 26 – 28, 2019). Note the different scale between panels.

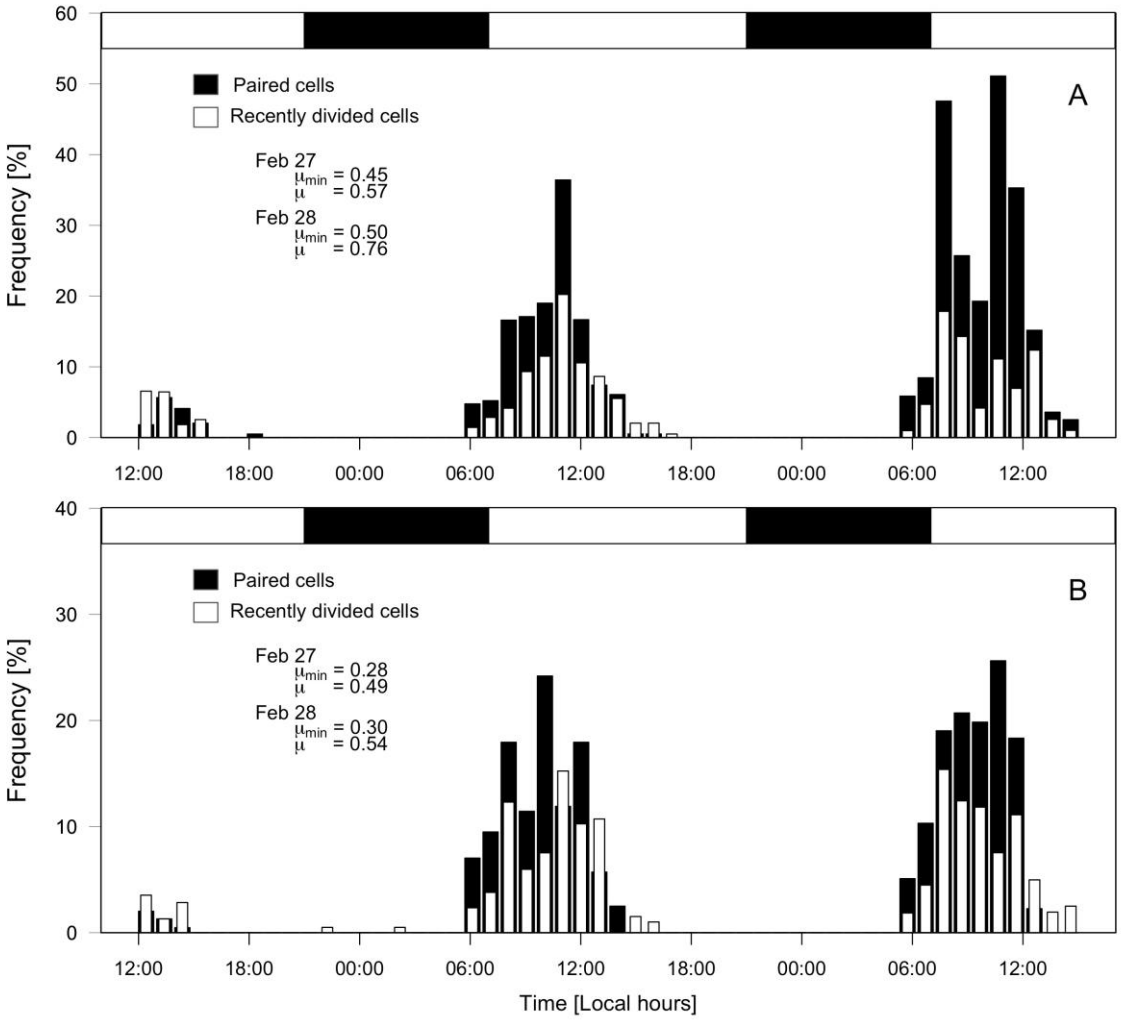

1217

1218 **Figure 7.** Cell cycle study, 26 - 28 February 2019. Distribution of frequencies (%) of paired
1219 (dividing, black bars) and recently divided (white bars) cells of: (A) *D. acuta*; (B) *D.*
1220 *acuminata* during a 48 h monitoring of cell cycle stages. Horizontal bar at top of graphs
1221 indicates period between sunset and sunrise. Note the different scale between panels.

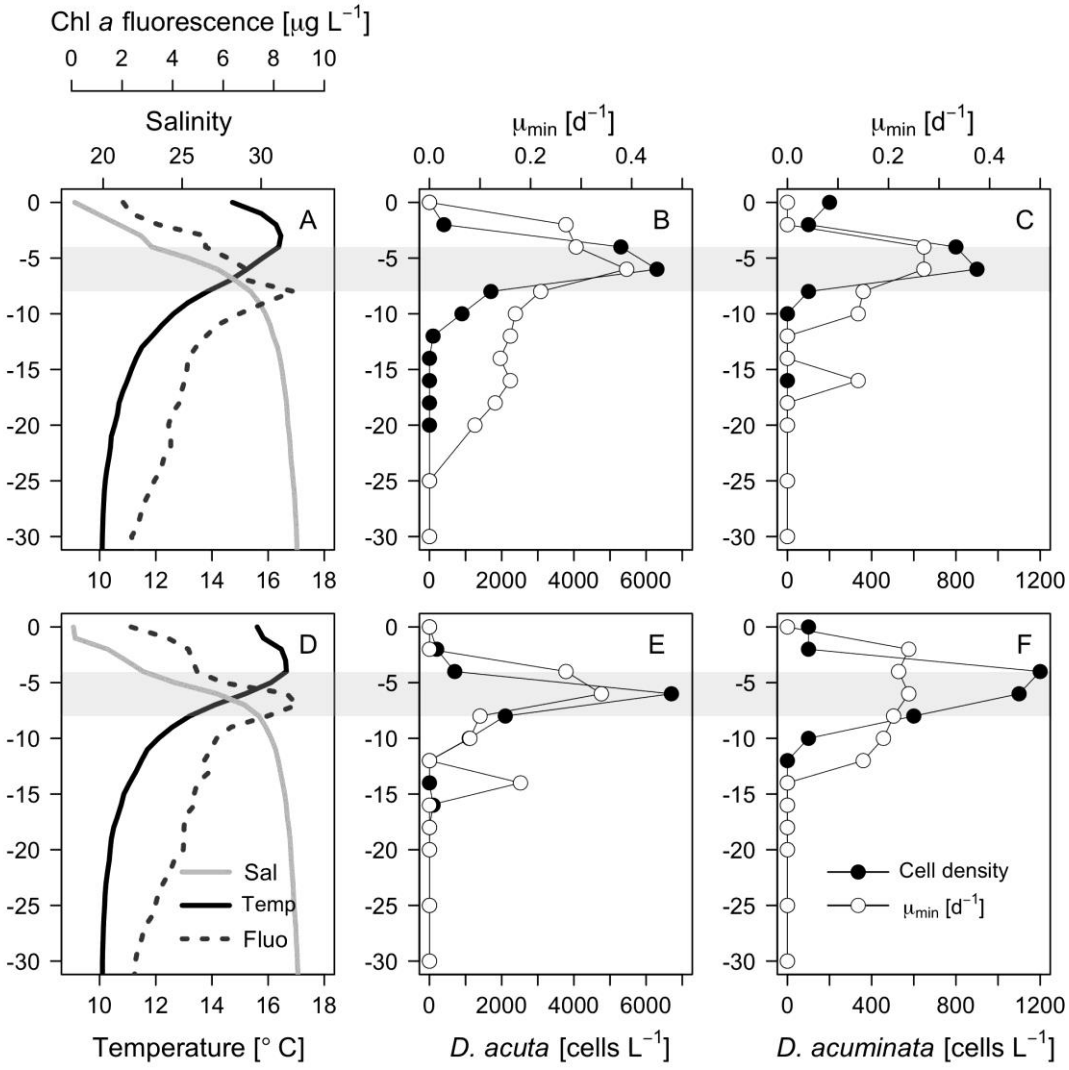

1222

1223 **Figure 8.** Vertical profiles of (A, D) Temperature, salinity and chl *a* fluorescence; (B, E)

1224 *Dinophysis acuta* and minimum division rate estimates at specific depths $(\mu_{min})_z$ (d^{-1}); (C,

1225 F) *D. acuminata* and minimum division rate estimates at specific depths $(\mu_{min})_z$ (d^{-1}) at

1226 10:00 h at the fixed sampling station on 27 February (top panels) and 28 February (bottom

1227 panels) 2019. The shadowed layer indicates the pycnocline position. Note the different

1228 scale between panels with *D. acuta* and *D. acuminata*.

1229

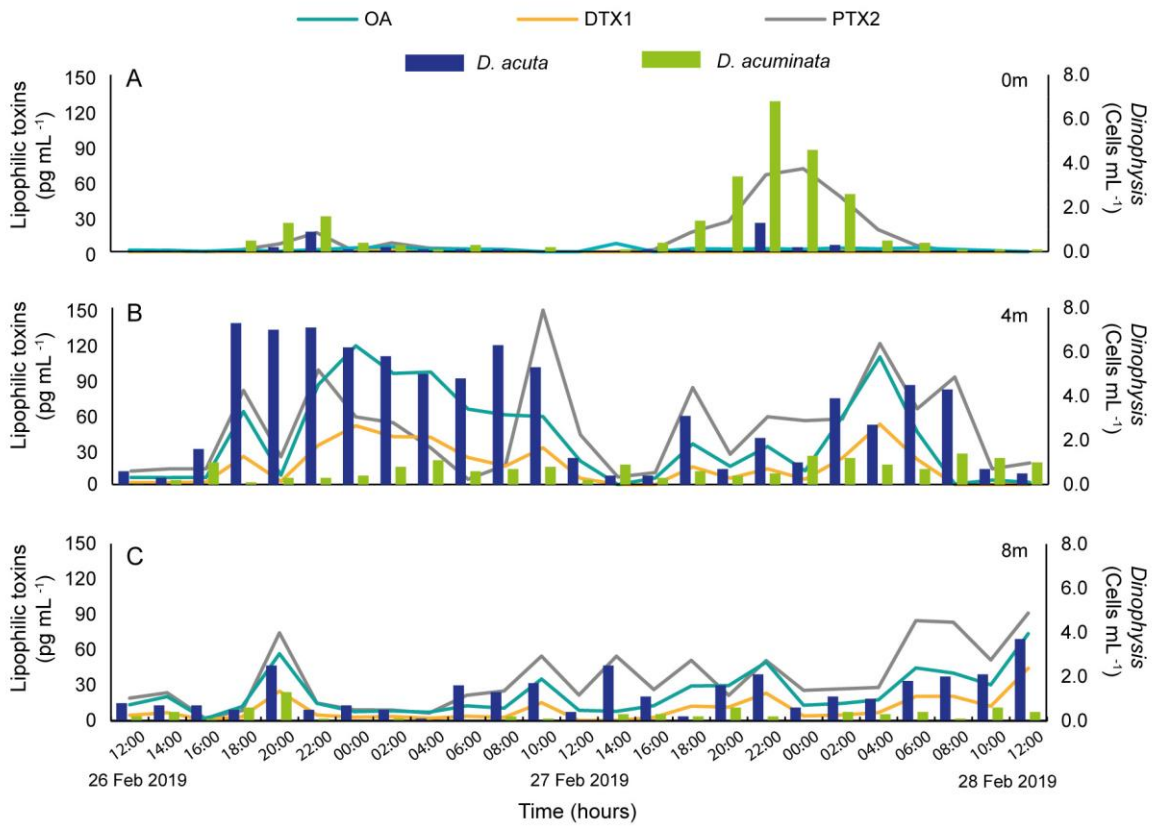

Figure 9. Distribution of lipophilic toxins concentration (pg mL^{-1}) in phytoplankton concentrates, and *Dinophysis* cell densities (cells mL^{-1}) at three depths: (A) 0 m; (B) 4 m; (C) 8 m, at the fixed sampling station during the 48 h study (February 26 - 28, 2019).

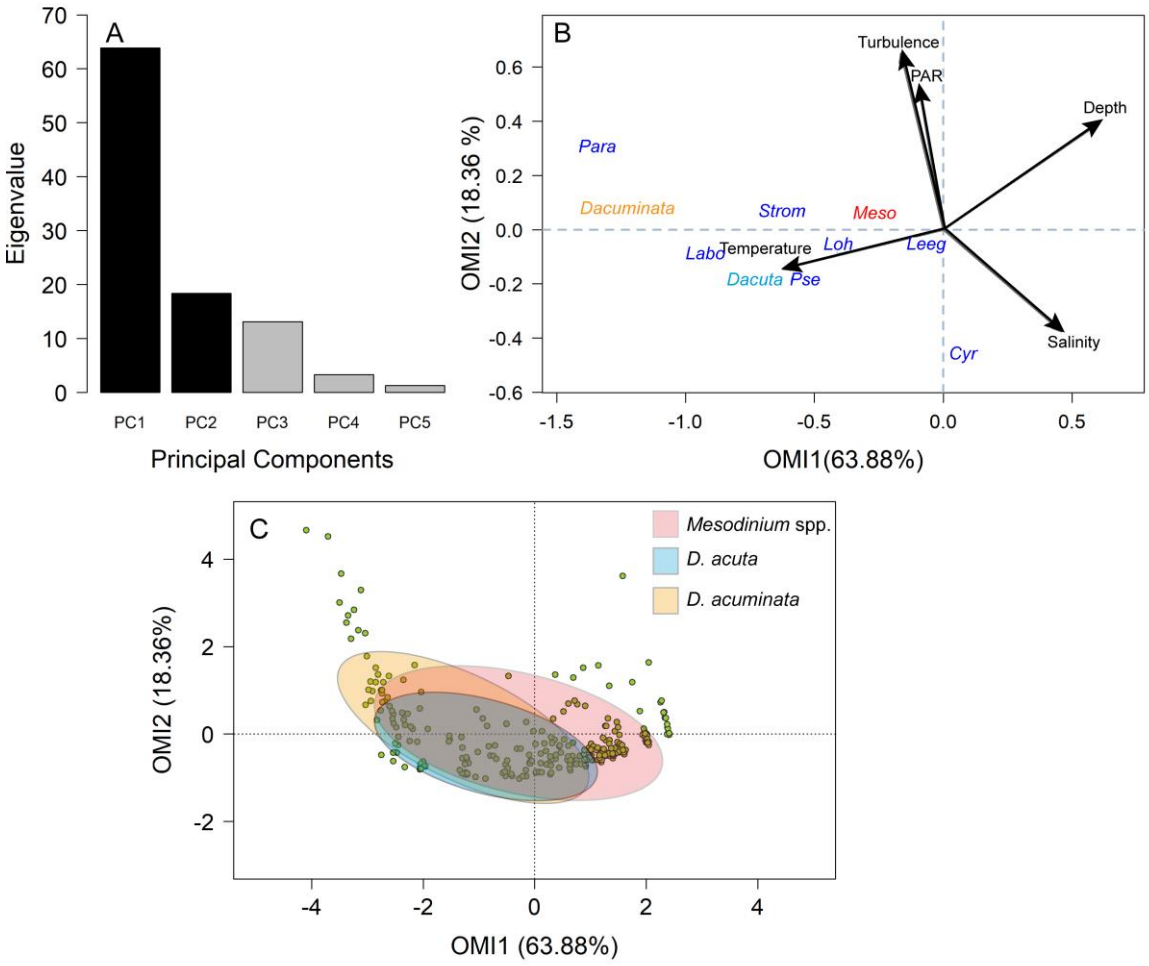

1234

1235 **Figure 10.** Outlying Mean Index (OMI) analysis of *Dinophysis acuta*, *D. acuminata* and
1236 co-occurring plastid-bearing micro-ciliates. (A) Bar plot of the eigenvalue in percentages
1237 of the total sum. Black bars are the chosen factorial axis PC1 (OMI1) and PC2 (OMI2);
1238 (B) Representation of the significant species' realized niche positions on the first two
1239 factorial axes with the canonical weights of environmental variables. The niche positions
1240 of *Dinophysis acuta* (light blue), *D. acuminata* (orange), their putative prey *Mesodinium*
1241 (red), and the ciliates (dark blue); (C) Realized niche breath of *D. acuta* (light blue), *D.*
1242 *acuminata* (orange) and the ciliate *Mesodinium* (red) found within the environmental
1243 space. Green dots represent the samples.